FTAS/TR-66-7

AN EXPERIMENTAL STUDY OF MELTING WAVE BEHAVIOR

by

Walter H. Edling and Simon Ostrach

June 1966

ABSTRACT

Following a survey of previous melting-wave studies, a flat-plate experiment is described which is designed to investigate the basic nature of waves formed on a melting body in a heated air stream. By varying material properties and ambient conditions, a range of values for a melting parameter, γ, is obtained, and the resulting wave behavior is recorded and analyzed.

It is found that the ratio of heating rate to softening rate (indicated by the parameter γ) is very useful in predicting the salient features of melting waves. By relating the data to this parameter and factors derived from the parameter, simple relationships are obtained to define wave velocity , amplitude, and spacing. A "critical" or minimum condition is also established for the appearance of the melt waves.

ACKNOWLEDGMENTS

The very necessary support for this study was provided by NASA Grant No. NsG-391/36-003-005.

TABLE OF CONTENTS

Chapter — Page

I. INTRODUCTION....1

Ablation Waves....1
Water Waves....6
Statement of the Problem....8

II. EXPERIMENTAL PLAN....10

Model Configuration....10
Control of Variables....11

III. TEST FACILITIES AND INSTRUMENTATION....14

Materials to be Melted....14
Wind Tunnel....18
Heating System....20
Test Plate....23
Cooling Bath....25
Instrumentation....27

IV. CALIBRATION AND PRELIMINARY TESTS....33

Tunnel Calibration....33
Effect of Varying Turbulence Level....36
Effect of Varying Plate Configuration....42
Measurement of Material Properties....45

V. TEST RESULTS....51

Critical Point....51
Ablation Data....59
Analysis of Results....63
Relationship to Original Problem....77
Summary....79

APPENDIX....81

Results from Chen's Analysis....81
Summary of Derivation of Ablation Parameters..83
List of Symbols....90

LIST OF REFERENCES....92

LIST OF TABLES

Table Page

1. Materials Used and Their Properties.....15
2. Conditions at Inception of Type 1 Wave Motion...55
3. Conditions at Inception of Type 2 Wave Motion...56
4. Ablation Test Conditions.....60
5. Ablation Test Results.....62
6. Parameters and Non-Dimensionalized Results.....66

LIST OF ILLUSTRATIONS

Figure — Page

1. Viscosity-Temperature Profiles--Pen 50 Asphalt, K-312 Resin, and #650 Oil.....16
2. Viscosity-Temperature Profiles--20W Oil and Glycerol.....17
3. Test Facility.....19
4. Instrumentation and Controls.....22
5. Plate Cross-Section.....24
6. Plate Plan View.....30
7. Velocity Profiles at Tunnel Test Section (Facing Downstream).....34
8. Effect of Varying Turbulence on Temperature Distribution.....38
9. Effect of Varying Turbulence on Wave Amplitude.....39
10. Effect of Varying Turbulence on Wave Velocity.40
11. Effect of Varying Turbulence on Wave Spacing..41
12. Alternate Plate Configurations.....43
13. Arrangement for Determining Thermal Conductivity.....48
14. Air Reynolds Numbers Required to Generate Waves in Various Liquids.....57
15. Plot of Non-Dimensional Wave Velocity Versus Ablation Parameter γ.....69
16. Plot of Non-Dimensional Wave Amplitude Versus Ablation Parameter γ.....72

17. Plot of Non-Dimensional Wave Spacing Versus Ablation Parameter γ.....75

CHAPTER I

INTRODUCTION

Ablation waves

For many years glassy stones have been found in certain locations on the earth including Southeast Asia, Australia, parts of the United States, the Ivory Coast, Bohemia, and Moravia. Called "tektites" and a variety of other names, these particles consist largely of SiO_2 in the form of silica glass and attracted attention because they differ markedly from the terrain in which they are found. As discussed by O'Keefe (1), the number of such particles is quite large in certain locations, but they are virtually unknown elsewhere. This fact and the dissimilarity between the tektites and local geological conditions has led to the proposal of many theories seeking to explain their origin and the method by which they were deposited on the earth.

One of the striking features of the Australian tektites is their shape. They appear to have been formed by partial ablative melting in a stream of hot gases from an initially spherical shape. The resulting button-shaped lump is covered with ring-shaped

waves encircling the stagnation point plus an accumulation of re-solidified material around the "equator" of the button. It appears that the material solidified originally in a spherical shape and was then remelted or ablated by passing through the atmosphere at high velocity.

Recent study has centered around this ablation behavior and has narrowed the range of theories to two of the strongest possibilities. Based on his extensive studies, Barnes (2) in 1961 supported the theory that the tektites are debris thrown up by the impact of a large meteor on the surface of the earth--possibly in Antarctica. More recently Chapman and his associates (3-7) and O'Keefe (8) have offered strong arguments which indicate that the particles consist of debris whcih was ejected from the moon by the impact of meteors on that airless surface and later captured by the earth.

The question of origin is an intriguing one, particularly to geophysicists; and the gathering of evidence continues. Recently O'Keefe (9) offered calculations based on the extremely low water content of tektites in support of the extra-terrestial theory of origin. He argued that it would be impossible to remove the large water content from terrestial material during meteorite impact without blowing the material apart

completely. Without entering directly into the discussion, other researchers (10-12) have determined additional information about the properties of tektites which may eventually contribute to the final determination of origin.

The approach used by Chapman in his attempts to determine the origin of tektites was based on attempting to determine the entry velocity and trajectories of the particles which display evidence of having ablated. After the discovery that an ablating layer of material can serve to shield an object in a high-temperature gas stream by absorbing heat during melting or vaporization and then flowing off the surface, considerable work in the field of ablation followed quickly. The application of ablative heat shields to re-entry vehicles served to stimulate research in this field; and by utilizing the theoretical results of Bethe and Adams (13), Chapman was able to draw his conclusions concerning approximate entry conditions.

Much of the early work in ablation (for example, references 14-19) was concerned with the fluid and thermal behavior of the ablating layer in the stagnation region. The important factors, of course, included the amounts of heat absorbed and transmitted by the shielding layer and the rate of erosion of the layer.

In the early works the possibility of waves or ripples on the surface of the ablating material was not recognized or investigated. In some of the arc-jet experiments used for ablation study, waves either were not present or were not discernible on the glowing liquid surface. The earliest theoretical studies were limited to the stagnation region, and no wavelike behavior of the melt was predicted.

Attempts to extend the work away from the stagnation region were initiated in limited form by Fanucci and Lew (20) and Tellep (21). In 1960 Ostrach, Goldstein, and Hamman (22 and 23) presented an analysis of the flow further around the body noting that the effects of deceleration become increasingly important as the flow direction becomes more parallel to the direction of the body forces. By scaling the basic equations, they showed that two basic parameters characterized the problem. One is essentially a reciprocal Froude number representing the ratio of deceleration to pressure (or viscous) forces; the other is governed by liquid properties and indicates the relative influence of convection and conduction. In addition, numerical integration of the basic equations indicated that deceleration forces could amplify a wave-like behavior of the liquid layer although such forces are not necessary for wave formation.

More recently, McConnell (24), in his Ph.D. research under the direction of Ostrach, expanded and improved the earlier results by applying a perturbation analysis starting from the initial state of conduction and a long-time analysis starting from time-independent ablation. He also performed experiments with asphalt spheres in a vertical, heated wind tunnel and obtained rather good correlation between the theory and the actual behavior. By varying the dynamic pressure in the vertical tunnel (with its constant body force), he was able to show that the reciprocal Froude number does indeed affect the wave behavior and that the numerical results obtained are quite reasonable. In conjunction with this work Ostrach and McConnell (25) predicted the existence of a "melting" parameter which in effect would give the relationship between the heating and softening rates for a body melting in a flowing gas stream.

In spite of the successes with these analytical results, a basic problem remained unresolved. The mathematical solutions as they stood did not take into account the coupling between the liquid layer and the gas stream flowing over it; and as a result certain limitations appeared. For example, the solutions predicted only a single wave during the melting rather than the series of waves observed in experiments. In the

solutions the outer boundary condition had been taken to be the known boundary layer flow over the initial body shape; hence changes in the gas flow caused by changes in the body shape or by a wavy surface were not reflected in the solutions.

In an attempt to improve this situation, Chen (26), in his work toward a Ph.D. degree at Case, has attacked the problem in a more complete form using not only the basic equations of the liquid layer but also the equations of the gas boundary layer. The resulting six equations are required to match at the gas-liquid interface in terms of shear, pressure, temperature gradient, and displacement normal to the interface. Work is still continuing on this obviously complex problem; however some basic parameters and reference quantities have already been obtained to characterize ablation behavior. These quantities are quoted in the Appendix; and as will be shown in this report, it appears that they are quite useful in predicting melting wave behavior. The basic parameter obtained in this work is a more general form of the one predicted by Ostrach and McConnell in reference 25.

Water waves

When considering wave behavior on a free surface such as that on a melting body, the investigator is

strongly tempted by the voluminous literature available on the subject of water waves (see, for example, the survey in reference 27). Indeed, such an approach is not to be ignored considering the obvious similarities. In the event that the mode of melting wave behavior is totally different than water wave behavior, there is still the reasonable possibility that both modes might appear--superimposed on one another--in either situation.

Chapman (4) noted the possible similarity between ablation waves and water waves; however there are also some differences. Ablation waves are generated in a material which is much more viscous than water and which contains very large viscosity gradients. It is generally known that water waves move much faster than the water itself; yet experimental results on melting waves do not reveal such behavior consistently. While Chapman obtained melting waves which did in fact move much faster than the liquid, seemingly contradictory results from McConnell's tests (24) indicated that liquid and wave velocities were of the same order of magnitude. It was at this point that Ostrach and McConnell (25) suggested that the variation in behavior might be related to the ratio between heating and softening rates, which was shown to be different for the two melting experiments.

Experimental work in the area of wind-driven

waves has largely been confined to low-viscosity fluids because of the obvious interest in ocean waves. Francis (28), however, obtained interesting results with a moderately viscous oil, which will be shown to be significant in light of the present investigation.

The study of film flow and film instability offers another possible guide to the melting wave problem. (See, for example, references 29 to 31.) The approach has been largely through the application of the Orr-Sommerfield equation and the principles of Kelvin-Helmholtz instability. The significance of these analyses will be discussed further in conjunction with the results of this project.

Statement of the problem

In light of recent developments it appears that significant progress is being made in the analytical treatment of the melting process. The practical application and verification of the proposed solutions have so far been confined to the data available from actual tektites plus the recent basic experiments of Chapman, McConnell, and Chen. Considerably experimentation has been completed in the development of ablative heat shields; however these investigations shed little light on the melting wave behavior since they were designed for different purposes.

The objective of this investigation, then, was to study experimentally the melting and ablation processes over a range of conditions with particular emphasis on the wave behavior. It was hoped that by varying the ratio between heating and softening rates through the parameter suggested by Ostrach, McConnell, and now Chen, the influence of these quantities on wave behavior could be established and perhaps the variation in previous observations could be explained. The project was undertaken to obtain a more broadly based understanding of the melting wave phenomenon to an extent not heretofore attempted.

CHAPTER II

EXPERIMENTAL PLAN

Model configuration

One of the fundamental decisions in any fluid dynamics experiment concerns the choice of physical configuration, with two basic approaches available to the investigator. Firstly, he might attempt to simulate a full-scale flow condition with a model hoping that proper scale factors or ratios can be found which will assure true similarity between the model and the real situation. Secondly, he can give up the restriction of a particular physical shape and instead attempt to obtain basic information using whatever shape is most convenient. Although the latter approach has a disadvantage in that the results may not be directly applicable to particular problems, it is ultimately more useful since such results sometimes can be modified to suit an individual problem or at least may be used to guide investigation and provide more detailed information about the problem area.

The second approach was chosed for this investigation since available basic data concerning melting

waves was rather sparse. The classical flat plate in a parallel air stream was chosen so that the effects of shape, curvature, pressure distribution, and gravity could be controlled or eliminated. In spite of simplifications afforded by the flat plate, another problem is created due to the difficulty involved in maintaining a truly flat surface as melting and flow begin. The approach to this problem is discussed in Chapter IV.

At the outset it was decided that the plate would be suspended in an air stream away from fixed boundaries to avoid established boundary layers. The top surface of the plate was intended to be the melting surface while the lower surface was to be insulated to prevent heating from below. Design details are discussed in Chapter III.

Control of variables

In view of the lack of well-established theory to predict melting wave behavior, it was not clear which variables and conditions would be most significant. From previous work the following were thought to have some effect:

1. Air stream Reynolds number.
2. Air stream temperature.
3. Air stream turbulence.
4. Air stream pressure gradients.
5. Body shape.
6. Gravity (or acceleration) parallel to the flow.
7. Physical properties of the melt.
    a. Softening point, Tm.

b. Specific heat, c_{pl}.
c. Thermal Conductivity, k_l.
d. Viscosity-temperature profile.
e. Prandtl number.

8. Reynolds number of the melt.
9. Initial body temperature.
10. Reciprocal Froude number of the melt.
11. Ratio between conduction and convection within the melt (Ostrach, reference 22).

Although several of the above quantities are interrelated, it is obvious that simultaneous investigation of all would be quite cumbersome. It was decided that the flat plate would be used in a horizontal position in a uniform, parallel air stream thus eliminating the effects of gravity, shape, and pressure gradients. For convenience the initial body temperature was held constant as was the free stream turbulence; although the effect of varying the latter was investigated briefly. The remaining items in the list are governed by the air velocity, the air temperature, and the material properties, which thus became the variables in this experiment. To accomplish the objectives, then, a wind tunnel facility was required with both velocity and temperature control; while a selection of different types of materials with varying properties was needed for the third variable. Separate study of each property and variable was not intended because of the large number of tests required. Instead, the dimensionless ratios or groups of the type suggested by Ostrach and McConnell (25) were intended to

provide a basis for systematic study of the results. As this project proceeded, the concurrent work by Chen (26) provided additional details for this approach.

CHAPTER III

TEST FACILITIES AND INSTRUMENTATION

Materials to be melted

The prime factor governing the choice or design of a suitable wind tunnel was the range of softening temperatures of the materials to be melted. To avoid the need for an elaborate high temperature facility, materials with low melting points were preferred; and preliminary investigation indicated that there are several types which have softening points near room temperature and which exhibit a steadily increasing viscosity with decreasing temperature rather than a distinct melting point. Those which were suitable included asphalts, petroleum oils, vegatable oils, glycerol, certain polymer resins, and silicone fluids. Ultimately 8 different materials were used including 5 for the actual melting tests. Table 1 contains a list of the materials used together with their physical properties. The viscosity-temperature profiles are given in figures 1 and 2.

Thanks are due to the Standard Oil Company and the Lawter Chemical Company for aid given in the form of material donations and information about physical

TABLE 1

MATERIALS USED AND THEIR PROPERTIES

Material	Supplier	T_m Softening Point ^oF	c_p Specific Heat $\frac{BTU}{lb\ ^oR}$	k Thermal Conductivity $\frac{BTU}{hr\ ft\ ^oR}$	ρ Density $\frac{Slug}{ft^3}$
Water[a]	--	--	--	--	--
Soyabean Oil[a]	--	--	--	--	--
Terlon 7 Resin[a]	Lawter Chemical Co.	--	--	--	--
#650 Oil	Standard Oil Co.	15	0.46	0.119	1.73
K-312 Resin	Lawter Chemical Co.	68	0.43	0.108	2.02
Pen 50 Asphalt	Standard Oil Co.	140	0.42	0.094	2.00
20 W Oil	Standard Oil Co.	-30	0.47	0.113	1.69
Glycerol	Fisher Scientific Co.	-25	0.58	0.170	2.43

[a]Used in preliminary tests only.

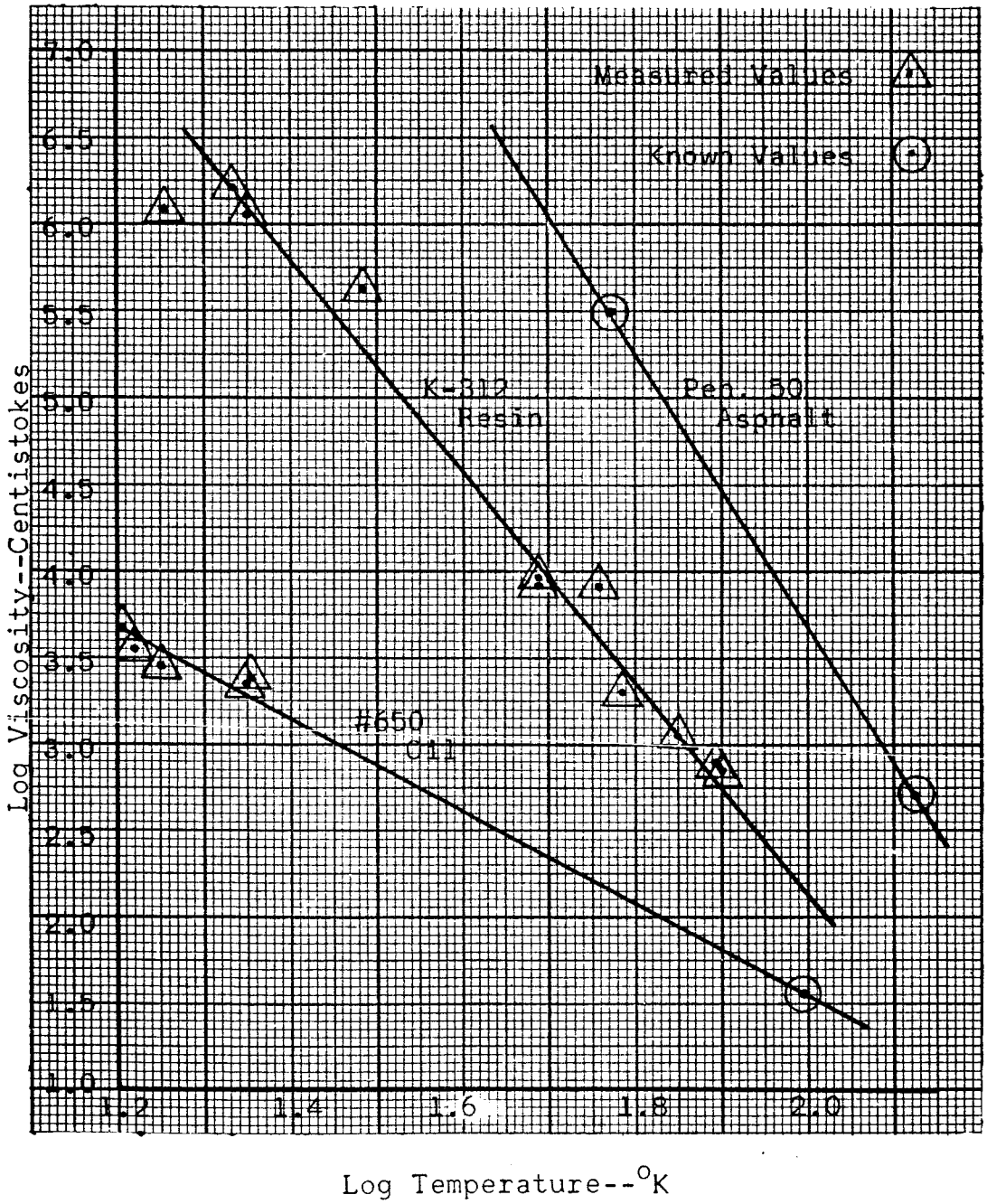

Figure 1--Viscosity-Temperature Profiles--Pen 50 Asphalt, K-312 Resin, and #650 Oil.

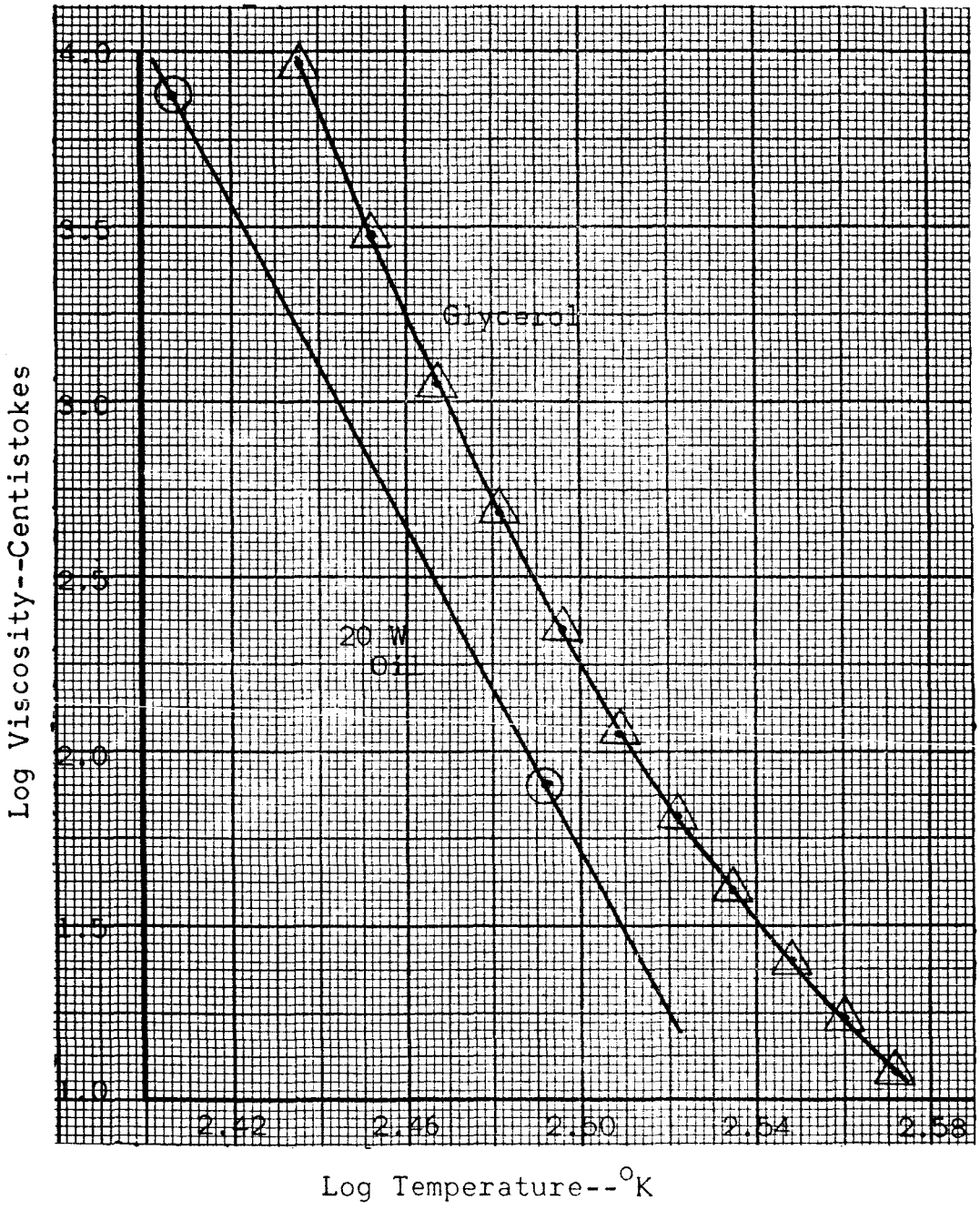

Figure 2--Viscosity-Temperature Profiles--20 W Oil and Glycerol.

properties. Where information was not available, direct measurements were obtained using methods described in Chapter IV.

Wind tunnel

For the available materials it appeared that a maximum air temperature of 200°F would be adequate for melting. Since high temperatures were not needed, an existing open-circuit wind tunnel in the Case Aerodynamics and Propulsion laboratory was used in conjunction with a finned-tube type steam heater. The flow in this tunnel is generated by a Joy Manufacturing Company axial-flow fan capable of generating air velocities from 0 to 125 feet per second at the test section. A vernier control, acting to vary the speed of a DC drive motor, permits velocity adjustment to within a fraction of one percent. The test section is 28 inches square and is accessible through a 20-inch square door.

To reduce the amount of heat required, only one quarter of the cross section (14 inches square) was used for testing. Plywood dividers were installed through the length of the tunnel to isolate the quarter section, and two doors were incorporated so that air flow could be diverted around the test section while the tunnel was in operation. Figure 3 represents the basic features of the arrangement.

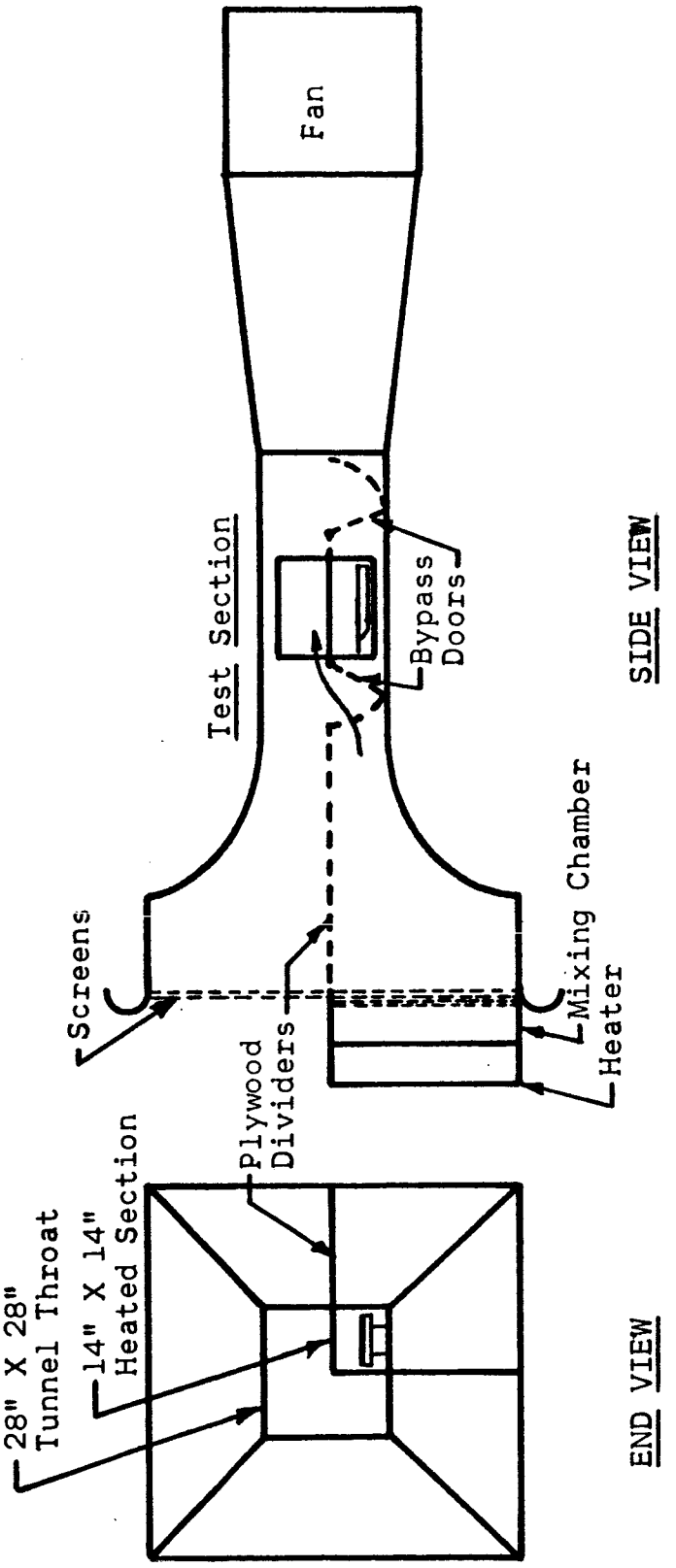

Figure 3--Test Facility

By using the bypass arrangement, it was possible to prepare the model outside the tunnel while the tunnel velocity and temperature were brought to equilibrium. The bypass doors were then shifted to re-direct the heated air to the unheated part of the tunnel while the model was being transferred from a thermal bath to the test area. After clamping the model in place, it was possible to start the test instantly by simultaneously opening the doors and starting the timer.

Heating system

Two standard Aerofin type 82 steam heating coils were used to heat the air entering the test quadrant of the tunnel. These units together cover a cross-sectional area of slightly more than 4 feet by 4 feet. Since the quadrant at the tunnel inlet is 49 inches square, it was possible to place the coils directly in front of the inlet screens. A mixing chamber was added later between the heater and the screens after difficulties were encountered with non-uniform temperature distribution.

Steam was chosen because of the large amount of heat required. A temperature of 200 ^{o}F at the throat with a velocity of 100 feet per second requires a heat input of nearly 1,000,000 BTU per hour, which is equal to the maximum design heating load for the entire

propulsion building in mid-winter. Electric power was not available in sufficient amounts, and gas fired units were avoided because of greater complexity. Steam condensing coils can readily convert this amount of energy if adequate steam flow and pressure are available. The steam supply in the propulsion laboratory is 50 psi, which corresponds to a saturation temperature of 281°F; therefore it would be possible to obtain temperatures in excess of 200°F by passing the air through several banks of coils and counterflowing the steam. In the actual tests only two rows of coils were used with a maximum air temperature output of about 180°F at 50 feet per second, which proved to be the limit for the present tests. At this temperature the plastic tunnel windows began to soften, and higher values would require a different facility.

Temperature control was obtained with a Robertshaw-Fulton thermostatically controlled valve in the steam supply line actuated by air pressure through a proportional temperature-sensing unit placed behind the plate in the free stream. With this system the temperature in the test section was controllable within $\pm 1^{\circ}$F and could be brought to equilibrium in about 10-15 minutes. As can be seen in figure 4, the sensing bulb was placed within the section between the bypass doors where it was not exposed to direct air flow when the doors were

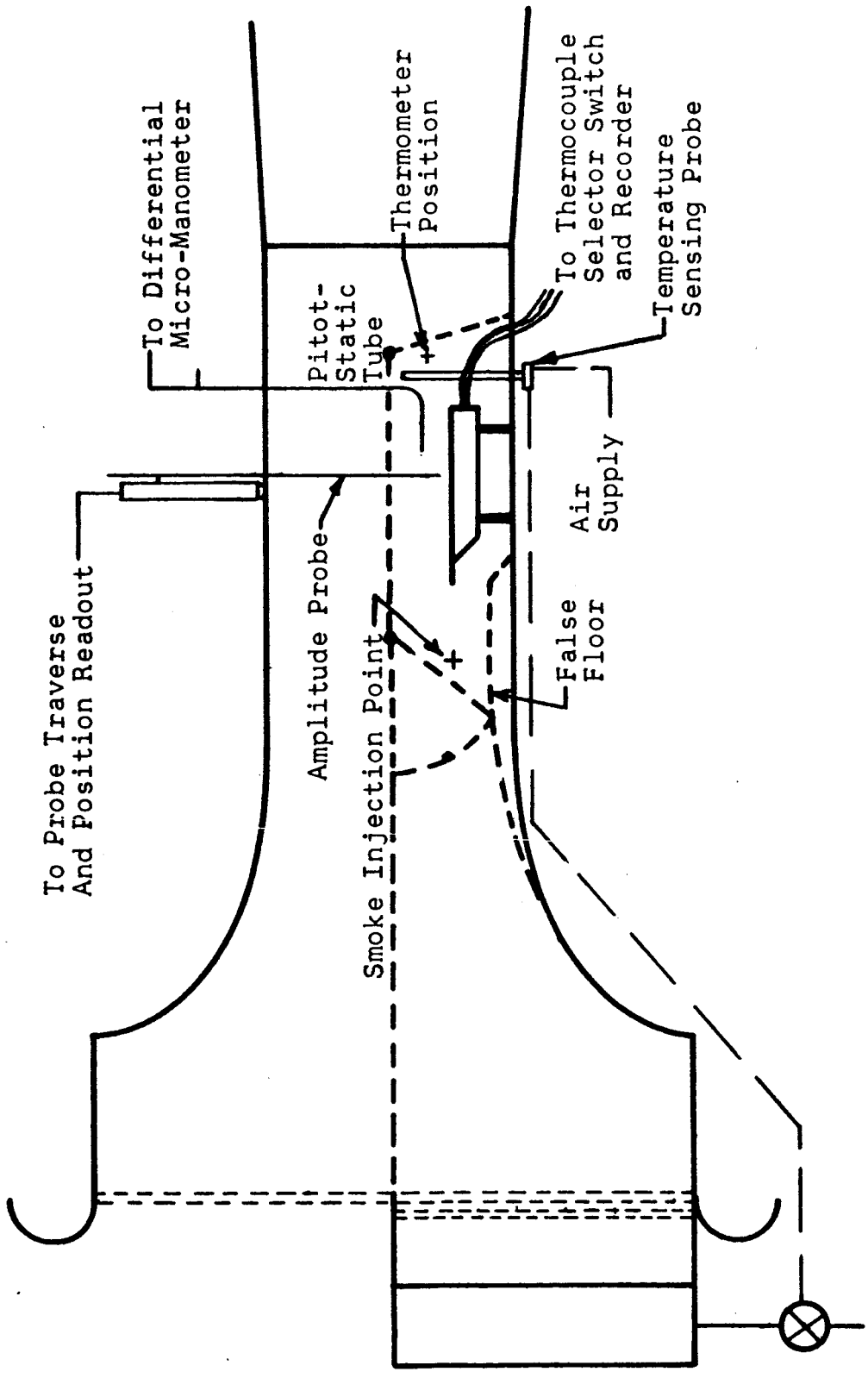

Figure 4--Instrumentation and Controls

in the bypass position. As a result the bulb tended to cool slightly while the model was being transferred into the tunnel, and the system temperature tended to rise in response. Loading time was about 30 seconds during which the temperature rose about 5-7°F at low temperatures and about 2°F at higher temperatures. After the air was turned back on, about 15-60 seconds were required before the overshoot was eliminated. Relocation of the bulb was not possible without placing it upstream from the model where it would create an undesirable disturbance. The effects of this variation are felt to be negligible and are discussed in Chapter IV with the results.

Test plate

The general configuration of the plate model used for the tests is shown in figure 5. It consisted of a flat piece of "G" grade acrylic (methyl methacrylate) plastic 1¼ inches thick, 15 inches long, 10 inches wide, tapered at the leading end, and fitted with a steel knife edge extending 1 inch beyond the plastic. Except for a milled pocket 10 inches long, 7 inches wide, and 1 inch deep which contained the material to be melted, the top surface of the plate was perfectly flat. The melted material was cast in place by pouring it into the leveled plate until it was even with the plate surface.

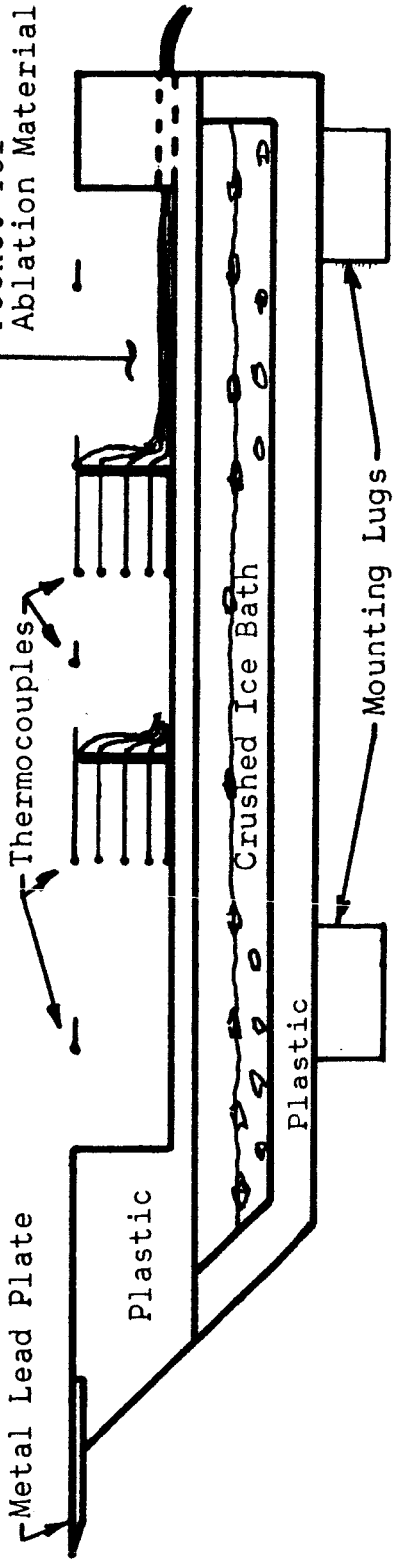

Figure 5--Plate Cross-Section

The plate assembly rested in the tunnel on another matching plate containing a layer of crushed ice. The layer of ice plus the stagnant air space between the lower and upper plates served to insulate the lower surface of the ablation model from the heated air. When in test position, the top surface of the plate coincided with the horizontal centerline of the heated quadrant of the tunnel.

The trailing edge of the lower plate was fitted with a narrow trough across its entire width to collect the melted material. It was found that the ablating material would flow to the rear edge of the plate and then follow the vertical back edge downward to the trough, which in turn was drained into a container on the floor of the tunnel. Very little material was lost into the tunnel during testing with this system.

The plate design used was the one selected after trying several alternative types. The ones rejected are discussed in Chapter IV as part of the preliminary tests.

Cooling bath

To extend the usable range of materials and to facilitate cooling the melted material after casting it into the plate, an isopropyl alcohol bath was used with powdered dry ice as the refrigerant. A metal tank

fitted into a large expanded plastic picnic cooler served as an insulated container. Temperature adjustments were made by adding more dry ice or warm alcohol as required. To eliminate one more variable, all tests were begun with the plate at -30°F, which was adequate to solidify all of the materials used.

Since most of the materials used are relatively insoluble in isopropyl alcohol, especially at low temperatures, little problem was encountered with contamination of the melting surface. However the glycerol used is very soluble in alcohol, and accidental contamination eventually necessitated rejecting two of the tests involving this material.

All materials with the exception of glycerol were totally immersed in the alcohol (after they had solidified) to speed the attainment of equilibrium. Initial solidification for all materials was obtained by having the lower surface of the plate in contact with the cold alcohol as the melted material was added. A supporting rack equipped with leveling screws permitted precise casting of the specimens directly in the bath.

Due to the low thermal conductivity of both the plastic plate and the ablation materials, approximately 3 hours were required to cast and bring a specimen to thermal equilibrium in the agitated bath. In the case

of glycerol, which could not be immersed totally, over 6 hours were needed to bring the whole specimen to equilibrium.

As the plate was transferred to the tunnel, most of the alcohol remaining on the surface drained off. The remaining alcohol was swept off within the first minute or less after the air was turned on.

Instrumentation

To follow the plan outlined in Chapter II, the following measurements were deemed necessary:

1. Air velocity
2. Air temperature
3. Air turbulence
4. Liquid interface velocity
5. Interface temperature
6. Temperature profiles within the body
7. Wave velocity
8. Wave spacing
9. Wave amplitude
10. Elapsed time

The instrumentation used to measure these quantities is shown in figure 4. Air velocity was held constant for a given test and was measured by means of a ¼-inch diameter pitot-static tube connected to a 30-inch Cox differential micro-manometer reading to 0.001 inches and filled with oil having a specific gravity of 0.827. The tube was attached to a traverse mechanism to permit the preliminary survey of velocity profiles in the tunnel. During tests the tip of the tube was located permanently 3½ inches above the top of the plate and 10

inches behind the plate leading edge. Barometric pressure was obtained from a standard, temperature-compensated mercury barometer located in the laboratory.

The air temperature was monitored continuously to the nearest $1^{o}F$ with a mercury-in-glass thermometer located 3 inches behind and 4 inches above the plate on the vertical center line of the tunnel. The preliminary temperature distribution was obtained with several thermometers at various locations in the tunnel cross-section.

Turbulence measurements were obtained using a DISA constant-temperature, hot-wire anemometer in conjunction with a Hewlett-Packard oscilloscope, which was used for calibration and study of turbulence forms.

To record information about wave velocity and spacing, a 16-millimeter movie camera with a 100-foot magazine was mounted outside the transparent tunnel door facing the plate from the side and top. Scales mounted along the plate edges provided length reference to the nearest 1/16 of an inch; while a digital timer reading to 0.1 second in view of the camera provided the time reference.

Initially it was hoped that liquid velocity could also be determined by introducing small paper chips on the liquid surface and photographing their progress. The method was only partly successful, and the

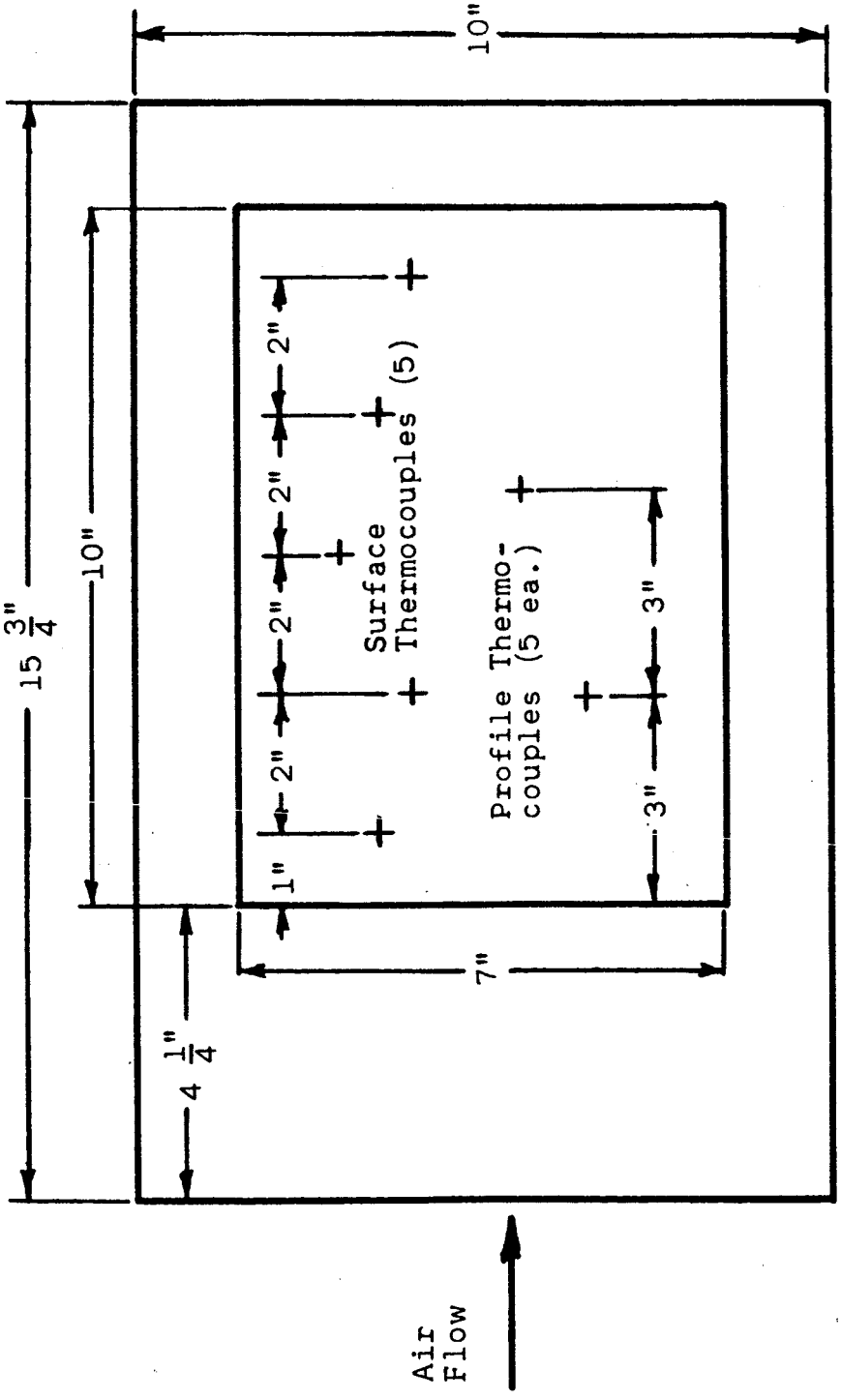

Figure 6--Plate Plan View

remaining 5 were placed flush with the original specimen surface at distances of 1, 3, 5, 7, and 9 inches from the front of the cavity. Small plastic supports were used to support and anchor the thermocouples since plastic has a thermal conductivity of the same order of magnitude as the melting materials.

To minimize the errors caused by thermal conduction along the thermocouple wire, the junctions were located 1 inch ahead of and at the same level as the support point. Since the temperature gradients in the horizontal direction are very small compared to the vertical gradients, this method served to minimize conduction by maintaining the immediate connecting wire at the same temperature as the junction.

The thermocouple leads were passed through the back edge of the plate, through the tunnel wall, and to a rotary thermocouple selector switch. A small DC motor was used to rotate the switch slowly so that each thermocouple was connected in repeating sequence to an ice-point reference and a Minneapolis-Honeywell recorder. Thus, the output of each thermocouple was recorded at intervals of about one minute on an 11-inch strip chart with a full-scale range of 4.00 millivolts or 169^{o}F. The thermocouple readings were synchronized with the film timer by marking the strip chart when the timer was started.

Thermocouple readings were used both for measuring temperature distribution during melting and for determining when equilibrium had been obtained in the cooling bath.

The data for each test, then, consisted of manual records of tunnel dynamic and static pressure, barometric pressure, air temperature, air turbulence, wave amplitude, initial plate temperature, and material type. The remaining measurements were taken from the motion picture films and the temperature strip charts.

CHAPTER IV

CALIBRATION AND PRELIMINARY TESTS

Tunnel calibration

After the tunnel had been modified by addition of plywood dividers, velocity surveys were performed in the test section to determine if the sectioning had produced any irregularities in the flow. Four vertical and three horizontal traverses were taken with the pitot-static tube. Velocity measurements at ½-inch intervals produced the map shown in figure 7. The deviations from the mean free-stream velocity amounted to ±1% or less to within 1 inch of the walls except on the side where the door was. Here the effect of the wall extended 1½ to 2 inches into the stream. Subsequent addition of turbulence screens and the finned-tube heater improved the velocity distribution somewhat. Final checks with the plate and all modifications in place indicated that the profiles were at least as good as those shown in figure 7, which were judged to be acceptable for the present tests. The model and sample outlines are shown on the map, and it can be seen that the melting material is well removed from

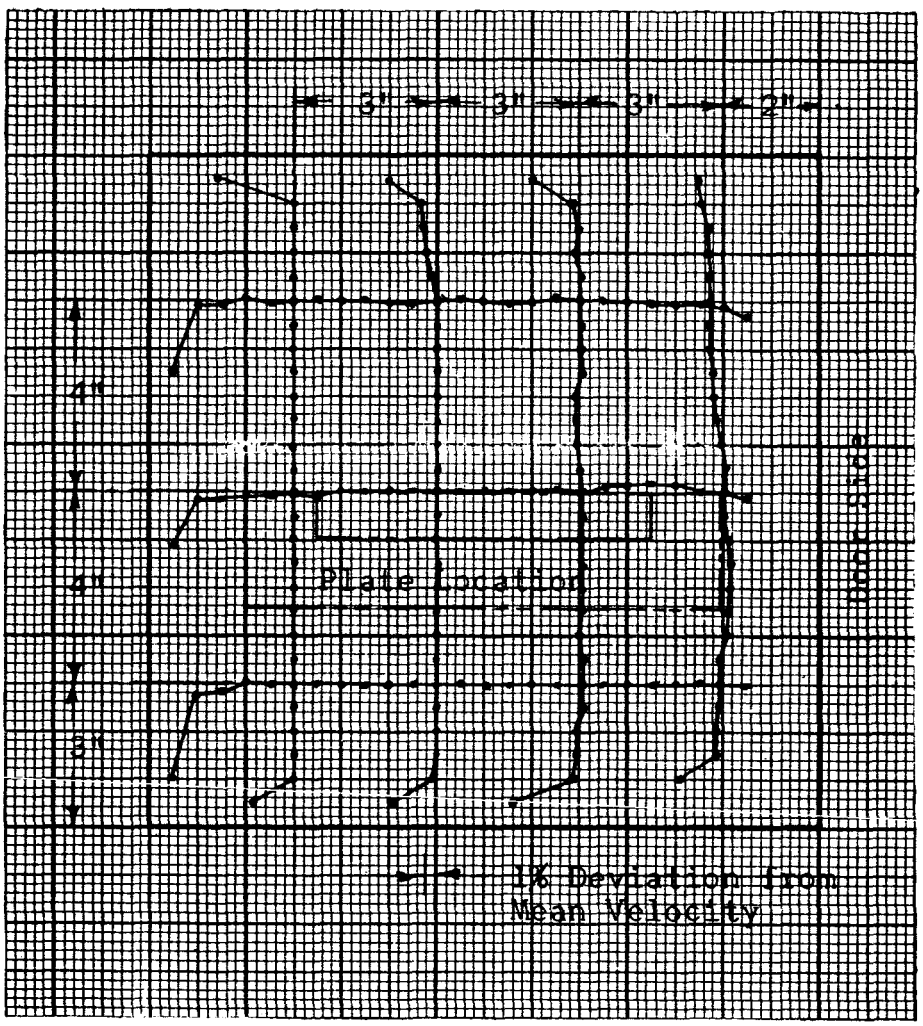

Figure 7--Velocity Profiles at Tunnel Test Section (Facing Downstream).

the wall effects.

The plate was installed in the tunnel with its top surface 7 inches from the floor or on the horizontal center line of the test section. Initial tests using smoke injected at the same level upstream from the leading edge revealed that the total mass flow was not dividing evenly as it passed the plate. Since the lower section of the plate containing the material pocket and the ice bath together with the mounting struts created considerable restriction in the lower half of the tunnel, more than half of the mass flow passed over the top of the plate. As a result the streamlines were deflected upward while in the region of the plate causing a flow pattern similar to fluid flowing over a plate inclined to the oncoming stream. The top surface of the plate was subjected to an eddying wake flow rather than parallel flow. To correct this condition, the floor of the tunnel ahead of the plate was raised until the mass flow between the floor and the center of the tunnel was exactly equal to that passing under the plate (see figure 4). Consequently, the flow in the upper half of the tunnel was exactly the amount passing over the top of the plate, and deflection of the streamlines was eliminated. Coarse adjustment of this false floor was accomplished by trial and error using the smoke injector. Smoke fed

into the stream ahead of the leading adge at plate level divided evenly at the knife edge when proper adjustment was obtained. A second check was obtained using the hot-wire anemometer placed in the plate boundary layer just behind the leading edge. As the false floor was lowered, the turbulence would increase suddenly when the wake appeared. Final adjustment was completed by raising the floor until the wake just disappeared. Some slight readjustment was necessary for each stream velocity used since the difference in resistance to flow over and under the plate varies with the Reynolds number.

When the steam heater coils were initially installed, the temperature distribution in the flow proved to be very erratic. The problem was remedied by inserting a baffled chamber between the heater and the turbulence screens which caused the heated air to mix thoroughly before entering the tunnel. After this modification, the maximum variation across the test section was $\pm 2^{o}F$, while the variation at a given point was $\pm 1^{o}F$.

Effect of varying turbulence level

As mentioned earlier, a DISA hot-wire anemometer was used to measure turbulence in the tunnel. Initially the tunnel produced a turbulence level of about 1.2 to 1.4% uniformly across the test section--values which

varied only slightly as the air speed was increased. In an effort to lower the level of turbulence intensity, two 70-mesh screens were added ahead of the existing screens. Although the value was lowered to 0.6%, it then became necessary to use the mixing chamber for the heater, which again raised the level to about 1.6%. Using reference (32) to predict the number of screens required indicated that to reach even the previous level of 0.6% would require six or more screens, which would seriously hamper the performance of the tunnel.

In an attempt to evaluate the need for turbulence reduction, two identical ablation tests were performed on a resin that would melt below room temperature. Since heat was not needed, it was possible to operate first with and then without the mixing chamber thus creating two turbulence levels, 0.6% and 1.6%. The two tests were compared with respect to temperature distribution, wave amplitude, wave velocity, and wave spacing. The results, which are plotted comparatively in figures 8 through 11, indicate that this change in turbulence is not particularly significant. Two tests certainly do not form a basis for general conclusions; however the results were taken as an indication that reducing the turbulence from 1.6% to 0.6% is of little value and that complete investigation of the effects of turbulence would require controlling the level to a truly

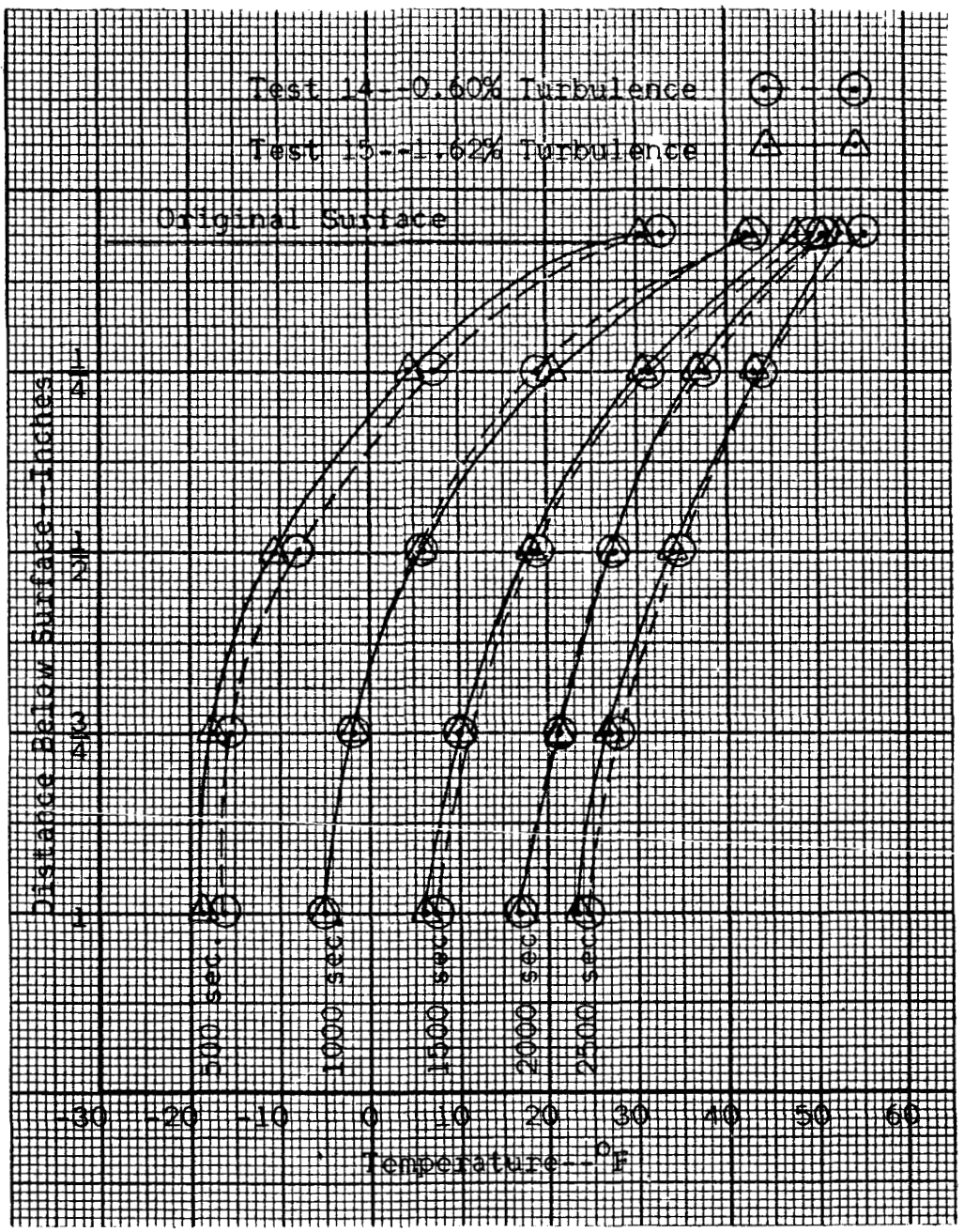

Figure 8-Effect of Varying Turbulence on Temperature Distribution.

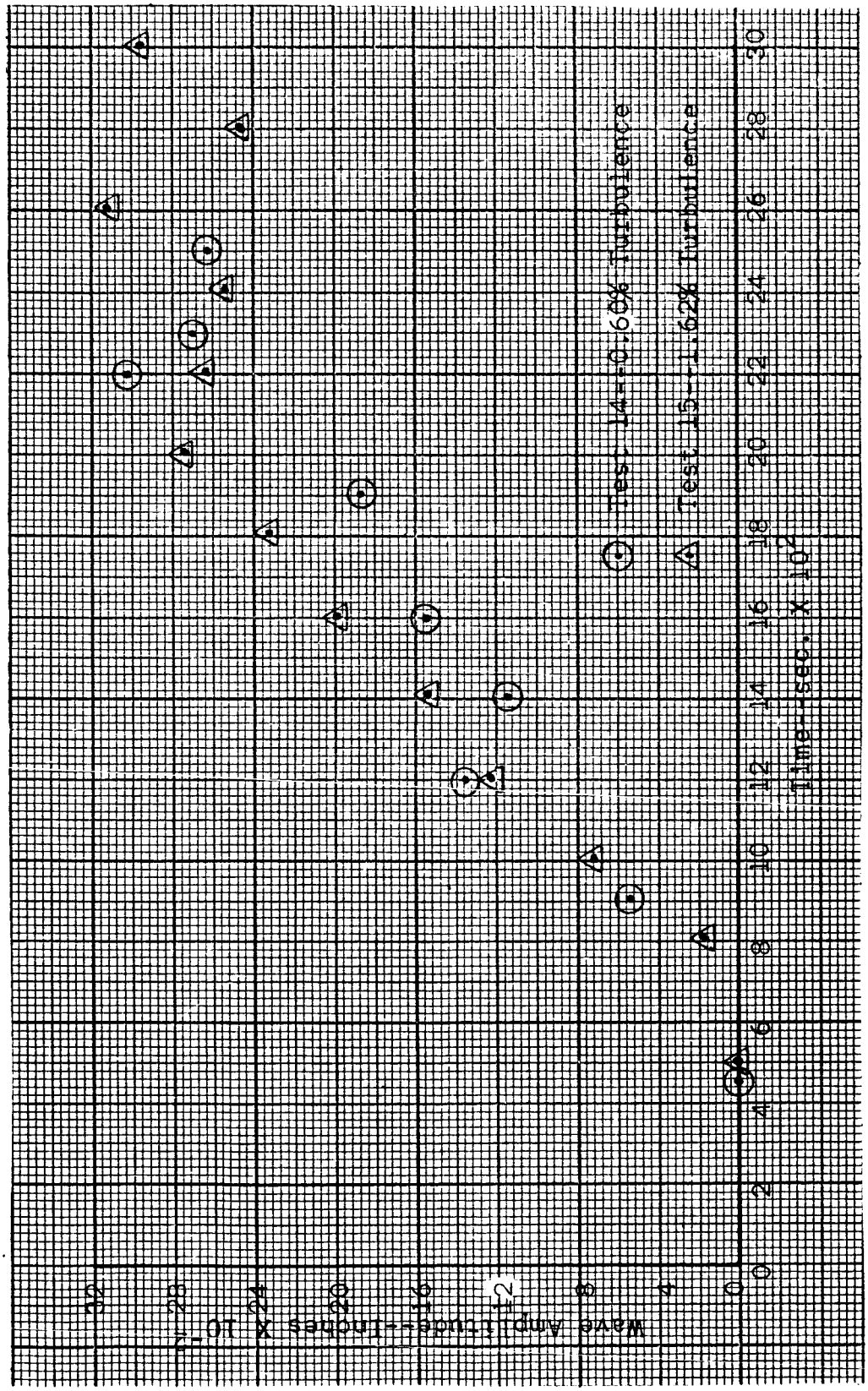

Figure 9--Effect of Varying Turbulence on Wave Amplitude

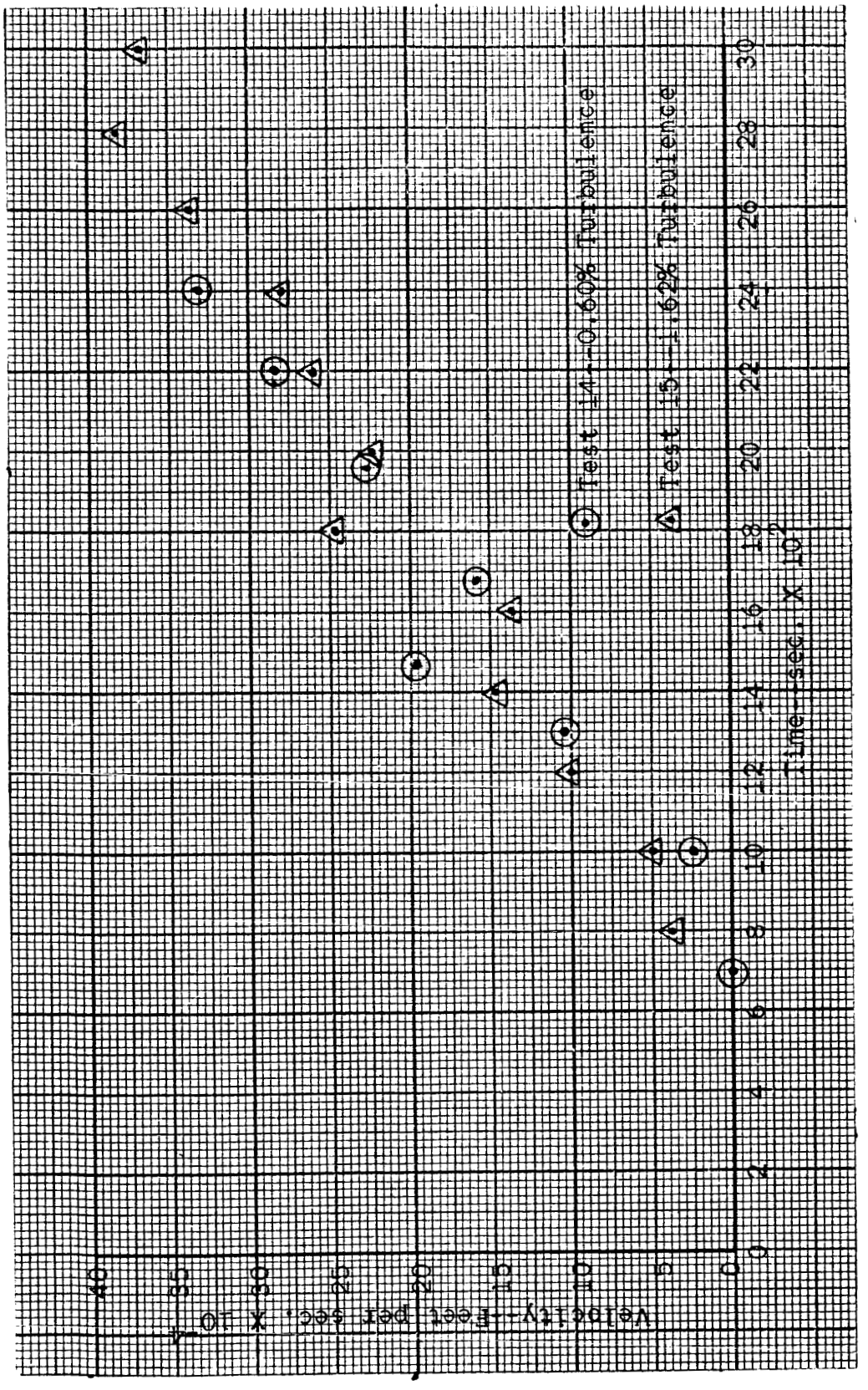

Figure 10--Effect of Varying Turbulence on Wave Velocity

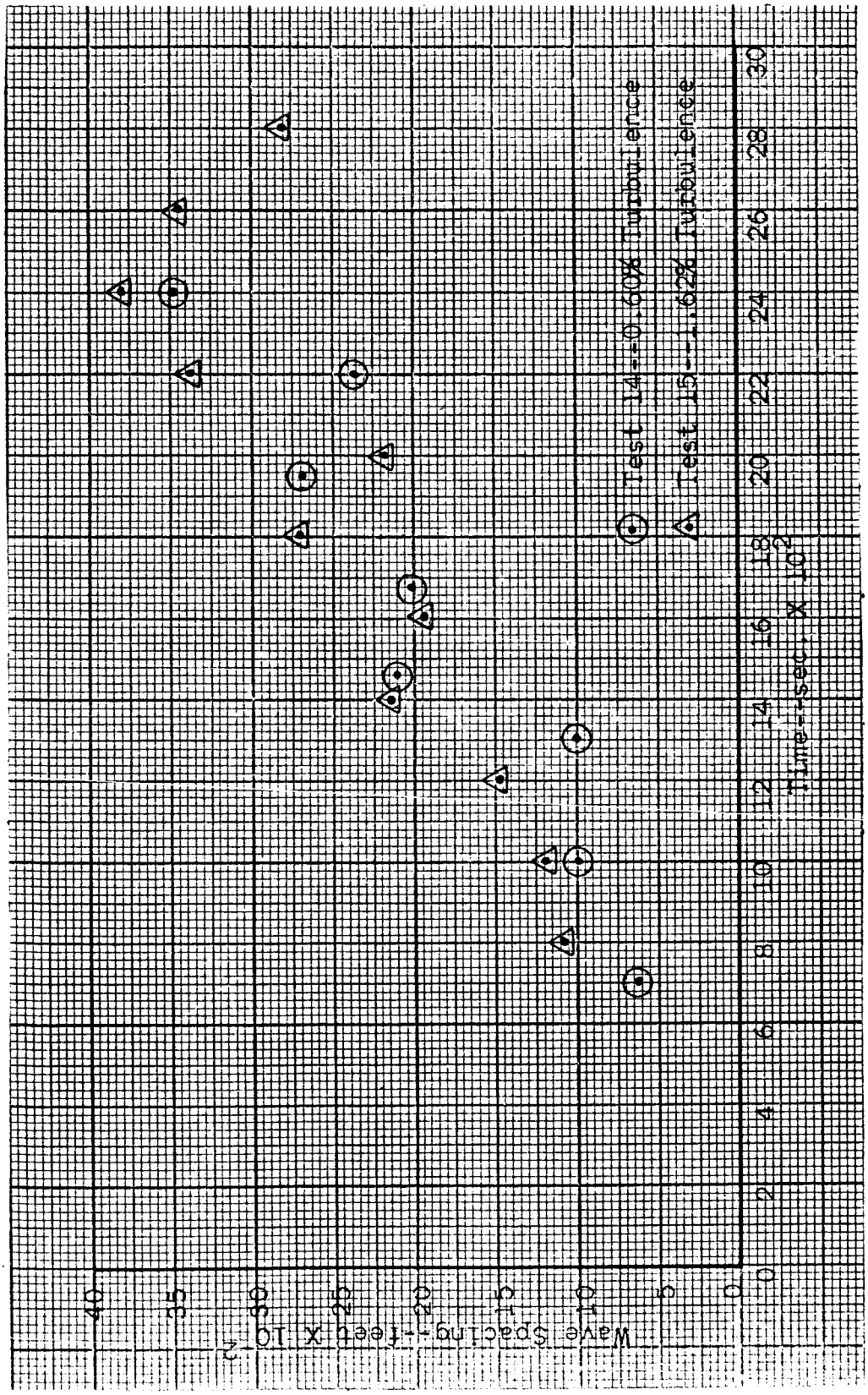

Figure 11--Effect of Varying Turbulence on Wave Spacing

low value--0.1% or less. Since such a level would have been very difficult to obtain without seriously restricting the performance of the tunnel, it was decided that the present tests would be carried out at the 1.6% level of turbulence.

Effect of varying plate configuration

The choice of plate configuration was made after considerable work. The theoretically simple, flat, thin plate becomes impossible in a melting process; it would simply melt and vanish in a very short time. Alternate approaches might be: (1) a uniform layer of ablative material on a flat, non-melting surface, (2) a tapering layer on a flat surface, and (3) a pocket of material sunken flush with an otherwise continuously flat surface.

The second alternative presents a problem in that it infers the existence of a wedge shaped layer of material which must be placed either with its original surface parallel to the flow or with the surface inclined so that the supporting plate is parallel to the flow (as shown in figures 12a and 12b). In either case there is no reason to believe that either configuration will approximate flat plate flow for even a short time.

The first suggestion seemed to offer possibilities based on the theory that the blunt leading edge of

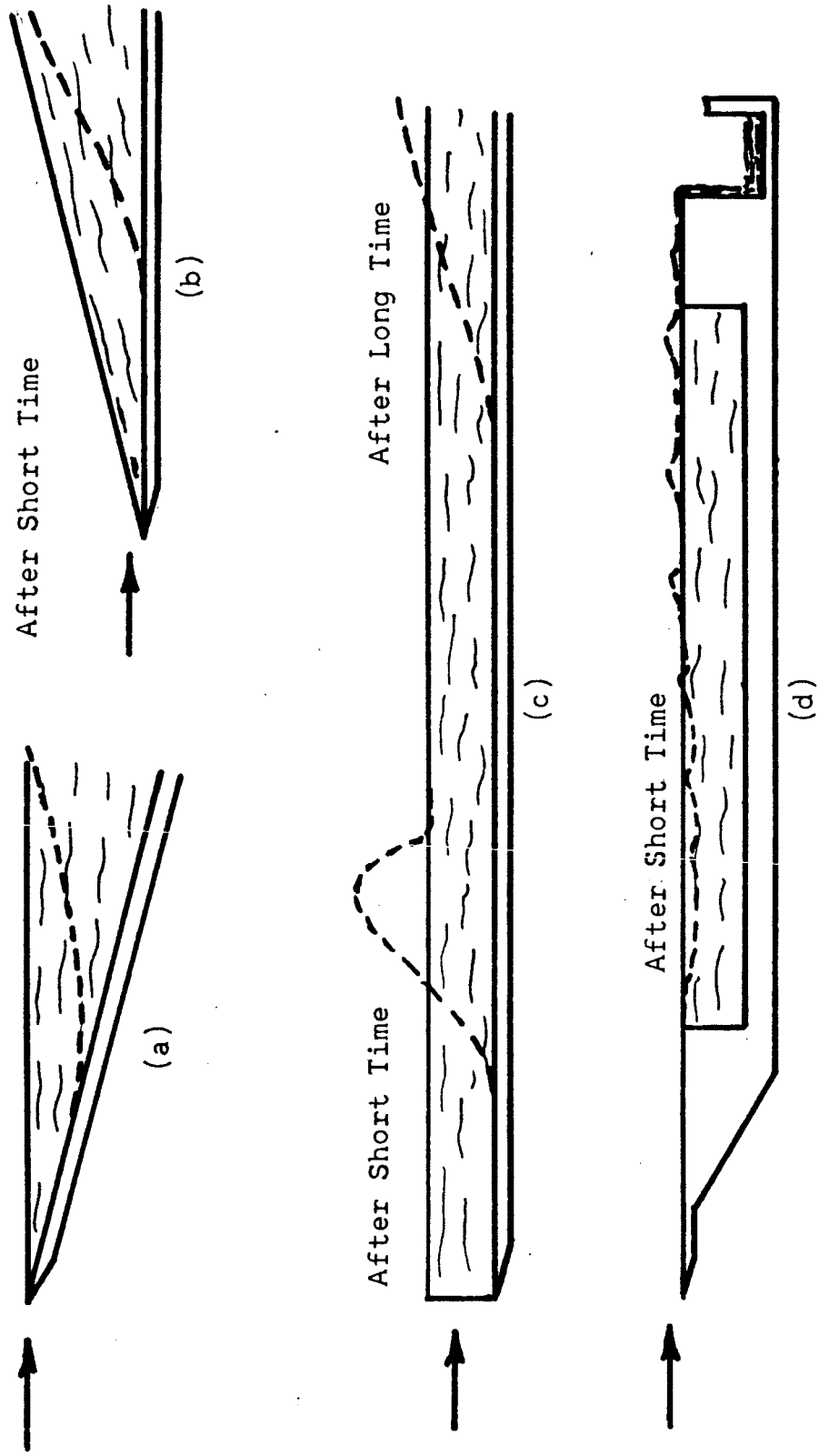

Figure 12--Alternate Plate Configurations

the melting material would break down rapidly and seek some sort of natural shape with a gently sloping "adjustment" region for the flow. However, when actually tried, this configuration resulted in the formation of a large roll of plastic material being formed as the entire leading edge area stripped away rapidly (figure 12c). Only after the "roll" had progressed over most of the plate did it subside into the desired natural shape, and by then most of the material was gone. This alternative was discarded because of the unpredictable behavior of the melting leading edge.

The third alternative was chosen, because it eliminated some of the difficulties of the other two and more nearly appeared to simulate flat plate flow. Preliminary tests revealed that material would melt first from the front of the pocket and tend to accumulate toward the rear (figure 12d). As steady state ablation was reached, the shape of the surface contained a slightly dished-out hollow immediately behind the solid leading surface occupying the first 3 to 4 inches of the pocket. The remaining 6 to 7 inches of material had a relatively flat surface covered with the waves, which traveled the length of the plate finally washing over the rear wall into the overflow trough. The maximum depth of penetration during the tests was about ¼ inch. Beyond that point the wave

character began to change noticeably indicating that the change in surface contour was becoming strongly significant.

This last plate design is obviously not a true, flat melting surface; but it was chosen as representing the best approximation to the desired shape.

Measurement of material properties

One of the more difficult problems faced was obtaining materials for which all required physical properties were known. It soon became evident that most of the desirable materials did not fall into this category. Reference 33 provided information for the asphalts used, and reference 34 gave the values for glycerol, although not necessarily at the correct temperatures. The Standard Oil Company provided some of the values for the oils used. After gathering these available values, the following properties remained unknown:

1. Density for the resins and for the oils at certain temperatures.
2. Specific heat for the oils and resins.
3. Thermal conductivity for the oils and resins.
4. Viscosity profiles for everything except for glycerol and one of the oils.
5. "Softening" temperature for everything. ("Pour point as quoted for some materials did not appear to be the correct measure for this condition.)
6. Surface tension for all materials except glycerol.

Complete, accurate measurement of these remaining quantities could have involved a great deal of time and

effort in itself unless reasonable tolerances were accepted. It was decided that measurements would be attempted with a permissable error of 5% or less.

The densities were obtained at two different temperatures using a set of standard floatation hydrometers, which are normally accurate within a fraction of one per cent. The possibility for some error lies in the fact that some measurements were taken at temperatures other than that at which the hydrometers were calibrated. Values of density at temperatures other than the measured points were obtained from a straight-line plot containing the measured values.

Viscosities were measured with a Fisher, Mac-Michael type, rotating-cup viscometer. When the Prandtl number of the sample is small (when the viscosity is small), it is possible to obtain values correct to within 1 to 2% with this instrument. Calibration against National Bureau of Standards oil samples verified this accuracy. At large viscosities, however, the accuracy suffers, because it becomes increasingly difficult to obtain uniform temperature distribution within the cup. Heat transfer depends largely on conduction rather than convection, and these materials have characteristically low thermal conductivities. The problem was aided by taking a number of measurements at various temperatures and plotting the results on log-log coordinates. A

straight line fitted to the points provided the necessary viscosity-temperature relation. It is felt that the final result meets the 5% criterion.

Specific heat was obtained by mixing known amounts of the sample and of hot water in a thermos bottle and measuring the equilibrium temperature. The heat content of the thermos and thermometer were obtained first by adding water alone. The value of specific heat was calculated by equating the heat given up by the water to the heat absorbed by the bottle and the sample. Initially this measurement proved to be the most troublesome. Errors in the measurement of known samples ranged as high as 15%. After more careful calibration and some practice, it became possible to keep the errors well within 10% on individual readings. Final values were taken to be the average of 3 tests to narrow the error to acceptable limits.

Thermal conductivity was measured by using the plate model itself with the addition of a metal pan filled with ice water on the top surface of the specimen and an additional thermocouple on the under side of the plate (figure 13). In this arrangement heat flowed downward from the ice water bath, through the unknown sample, through the plastic plate, and into the alcohol bath. Since the plate was nearly 10 times as wide as it was thick, heat flow in the horizontal

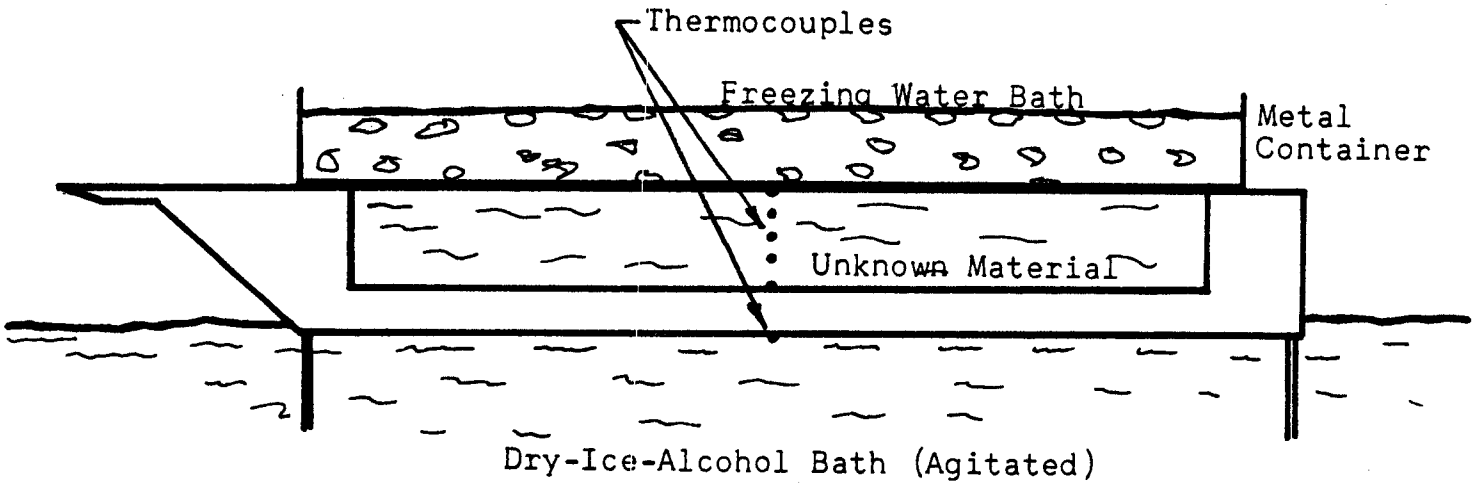

Figure 13--Arrangement for Determining Thermal Conductivity

direction was taken to be negligible. The thermocouples placed at the surfaces of the sample and the plastic as well as at the interface provided measurements of temperature gradients across each layer. After equilibrium had been obtained, the gradients were measured; and since the thermal conductivity of the plastic was known, direct calculation of the sample conductivity was possible by equating the heat flows through the two layers. The value for the plastic was supplied by the manufacturer and verified by calibration against a known material (glycerol). In spite of the crudeness of the method, further tests on known materials (asphalt) yielded results well within the 5% limit of error established earlier.

The values of "pour point" furnished by manufacturers proved to be different from the observed "softening" point as applied to the onset of ablation. It was discovered that materials would begin to flow and form waves at temperatures somewhat lower than the quoted pour point. A seemingly more indicative measurement was obtained by slowly cooling a sample of the material in a two-inch diameter container while stirring it with a thermometer. The temperature at which the material failed to flow when the container was suddenly inverted was taken as the "softening" point. Several trials were used to determine an average for each

material.

For preliminary tests the surface tension of the materials was needed at a temperature of 72°F. Values were obtained using a Fisher "tensiomat" instrument which is readily capable of producing the required 5% accuracy.

The values obtained from the above procedures are limited by the tolerances accepted. Furthermore, the effects of changing temperature on specific heat and thermal conductivity are not directly known. The specific heat was measured at an average temperature of about 100°F and is assumed constant even though it does vary slowly with temperature. The thermal conductivities obtained are essentially average values over the range from 32°F to about -50°F because of the method used. Although thermal conductivity does vary considerably with temperature, the measured value is accepted since it falls roughly within the actual temperature range encountered by the material during the tests.

Due to the tolerances and the above assumptions, the information about physical properties must be accepted as being perhaps the most serious source of possible error in the tests.

CHAPTER V

TEST RESULTS

Critical point

During calibration and preliminary testing, an interesting phenomenon was noted in regard to the behavior of melt waves. It appeared that below certain air velocities no waves would form whatsoever even though the material was completely melted. Since this fact would obviously affect the approach to the actual ablation tests, some preliminary experiments were performed using both frozen and unfrozen liquids of several types in an effort to study this apparent critical point.

Initially the results were very confusing. Five liquids ranging from relatively low viscosity types (water) to very high viscosity types (resin) were used in the plate model without freezing and with the air stream at room temperature. The stream velocity was increased slowly until some type of wave or ripple was noted. At this point the air velocity, wave velocity, and wave length were recorded manually and on motion picture film. An attempt was also made to measure

liquid surface velocity; however it was not too successful.

The tests on three of the more viscous materials yielded one type or mode of wave behavior which began at approximately the same air speed for each material (an average of 31.8 feet per second). This type of wave appeared first at the front edge of the liquid specimen beginning as a stationary hump or ridge at air speeds below the critical value. As the air speed was increased, the height of the hump increased, and the slopes of its sides became steeper; then, at a well-defined and repeatable air speed, it began to move downstream. As the first ridge or wave began to move, a second one formed in its place at the leading edge. When the second one reached full height, it too began to move; but as it did, the first one slowed almost to a stop and shrank rapidly, disappearing in a short time. By increasing the air speed somewhat more, it was possible to drive the waves farther along the plate until they reached the back edge without stopping.

The two fluids tested with lower viscosity (water and light oil) displayed a much different behavior. The first waves to be noticed were ripples which appeared near the downsteam end of the plate. These ripples occurred at air speeds of 18 and 25 feet per second respectively, which are somewhat lower than the

speeds required to generate a wave on the more viscous materials. Furthermore, the ripples did not form and grow in the same manner as the other waves, which appeared at the leading edge first; but rather they appeared simultaneously over a large area. Considerable fluid motion was noted at the interface before the appearance of the ripples.

Increasing the air speed further produced a most interesting situation. At a value approximately equal to the 31.8 feet per second mentioned previously, a second type of wave appeared to engulf the existing ripples. This second type behaved in a similar fashion to the type observed on the very viscous liquids, was higher, moved more rapidly, and completely obliterated the smaller ripples. The velocity of the first type of ripple was significantly greater than the liquid velocity, while the second type of wave appeared to transport fluid at its own velocity. Paper chips on the surface rose and fell as the first type of wave passed; but when the second type occurred, the chips were picked up and immediately washed over the back edge of the plate.

The occurrence of two distinct types of wave behavior has been noted before in the literature. Francis (28) observed two distinct wave types in his study of air flowing over oil--types which were very similar to the ones seen here. Dukler (35 and 36), in studies of

annular film flow on vertical tubes, observed two changes in wave behavior as did Knuth (37) in his work with horizontal ducts.

To examine the significance of the two types of waves obtained here, it is helpful to summarize the conditions existing when each type is first noted. Table 2 lists the material properties and the conditions prevailing when the first wave (called type 1) was first seen on the low-viscosity liquids. Table 3 contains similar information for the second type (called type 2). Since the waves observed on the viscous liquids seemed to be of the latter type, they are incorporated into Table 3. The result obtained by Francis (28) is also incorporated at the appropriate places.

The most significant parameter to note is the air Reynolds number existing at the inception of each type of wave. These have been plotted against the liquid viscosity in figure 14; and as can be seen, the type 2 wave seems to occur at a relatively constant value of the air Reynolds number. Furthermore, since the liquid viscosity is essentially related to the liquid Reynolds number, it can be said that the type 2 wave is independent of the liquid Reynolds number. (The variation in liquid velocity was small compared to the variation in viscosity; hence the Reynolds number is governed by the viscosity.)

TABLE 2

CONDITIONS AT INCEPTION OF TYPE 1 WAVE MOTION

	Water	Soybean Oil	Mineral Oil[a]	Glycerol	#650 Oil	K-312 Resin
Viscosity C'stokes	0.94	68.0	251	810	2,320	725,000
Surf. Ten. dynes/cm.	72.3	32.9	34.0	63.2	32.0	37.6
Density g/cm^3	0.998	0.918	0.875	1.260	0.895	1.040
Airspeed ft/sec	18.25	25.60	31.70	---	---	---
Air Reynolds No.[b]	$3.95X10^4$	$5.53X10^4$	$6.86X10^4$	---	---	---
Wave Vel. ft/sec	0.585	0.701	0.030	---	---	---

[a]From reference (28)

[b]Based on the distance from the plate leading edge (4.25 inches).

TABLE 3

CONDITIONS AT INCEPTION OF TYPE 2 WAVE MOTION

	Water	Soybean Oil	Mineral Oil[a]	Glycerol	#650 Oil	K-312 Resin
Viscosity C'stokes	0.94	68.0	251	810	2,320	725,000
Surf. Ten. dynes/cm	72.3	32.9	34.0	63.2	32.0	37.6
Density g/cm^3	0.998	0.918	0.875	1.260	0.895	1.040
Airspeed ft/sec	33.9	27.8	31.7	33.4	29.1	32.8
Air Reynolds No.[b]	7.37×10^4	6.05×10^4	6.86×10^4	7.21×10^4	6.29×10^4	7.09×10^4
Wave Vel. ft/sec	(c)	0.962	2.25 (est.)	0.366	0.032	4.20×10^{-4}

[a]From reference (28).

[b]Based on the distance from the plate leading edge (4.25 inches).

[c]Could not be measured.

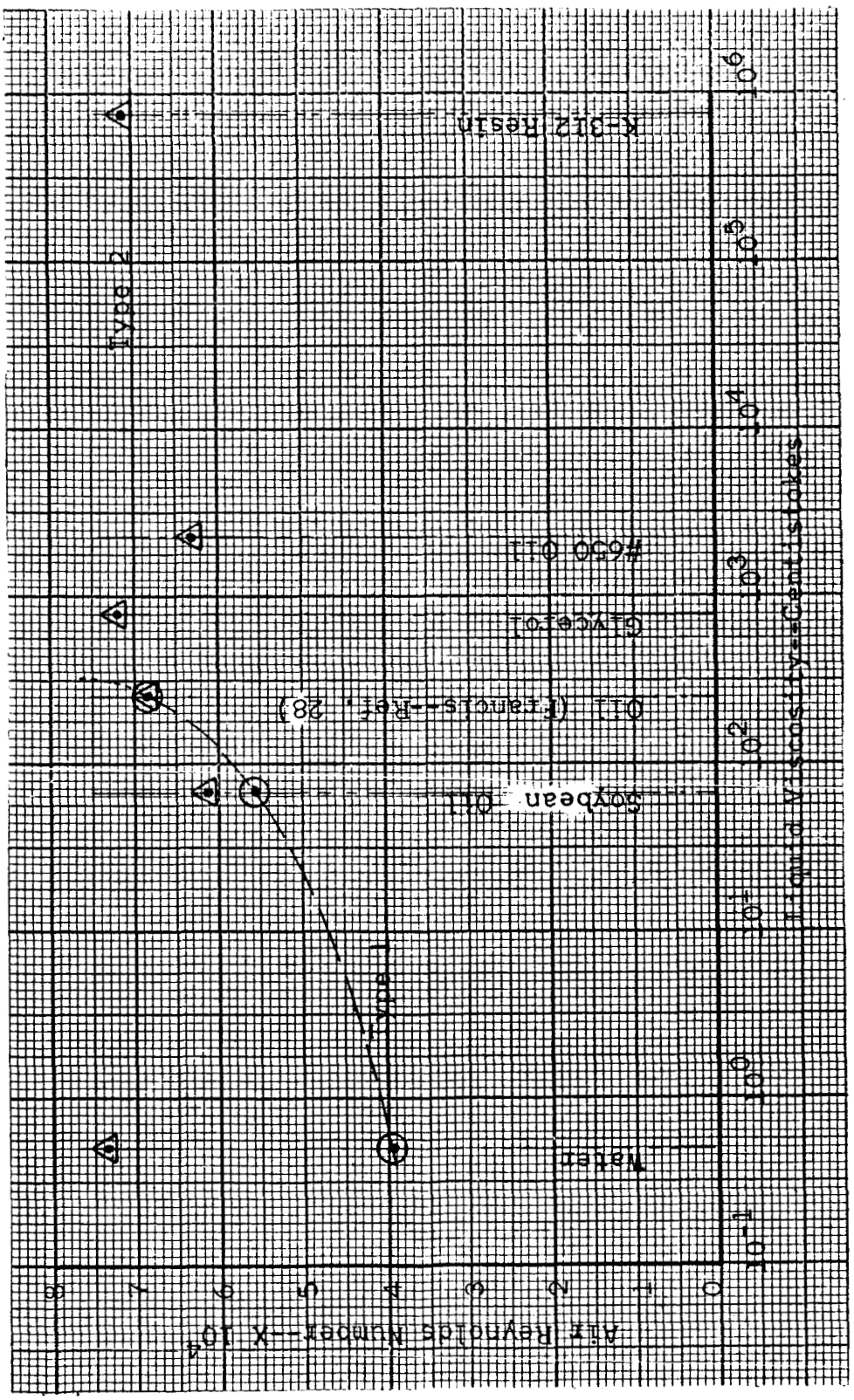

Figure 14--Air Reynolds Numbers Required to Generate Waves in Various Liquids

Comparing these conditions to the various types of instabilities described by Ostrach and Koestel (29), it would appear that this behavior is possibly of the Kelvin-Helmholtz variety, which is caused by the interaction of two unlike fluids in relative motion at their common interface. The dependence of this type of wave behavior upon the gas Reynolds number is in agreement with the observations of Dukler (35 and 36) and Laird (38), both of whom noted a similar dependence.

Again referring to figure 14, it can be seen that the type 1 waves do appear to depend on the liquid viscosity and the liquid Reynolds number. These waves were observed in liquids which displayed relatively large liquid velocities in conjunction with low viscosities (i.e., large Reynolds numbers) and were absent in the more viscous fluids. The apparent dependence on the liquid motion points to the Tollmien-Schlichting type of instability (reference 29), which derives its existence from amplification of disturbances within the liquid layer (i.e., transition). This behavior agrees with other observations by Kinney, Abramson, and Sloop (39); Brauer (40); and Knuth (37); all of whom found a dependence of waves upon liquid motion under certain conditions.

Although the type 1 waves were not observed in the more viscous liquids, there is no reason to believe

that they would not form if the air velocity were increased sufficiently. Since the larger, type 2 waves appear before this point is reached, the occurrence of type 1 waves is either masked or prevented by the radical distortion of the surface.

While these few trials are not meant to be taken as being conclusive, the pattern is very significant since the "ablation" or "melt" waves measured in subsequent tests are evidently equivalent to the type 2 phenomenon. The form and behavior of the melt waves were found to be very similar to this type, and it was discovered that waves would not form on ablating surfaces unless the air Reynolds number exceeded the minimum value established for type 2 waves.

Ablation data

A total of 32 complete ablation tests were performed using the procedures outlined earlier. Table 4 contains the summary of test conditions exclusive of the material properties, which have been given in table 1, and the properties of air, which were taken from reference 41. Test number 54, using paraffin, proved to be useless as far as wave data is concerned. Paraffin has an actual melting point rather than a continuous softening range; and it was used for comparison to the other materials. Very small ripples formed on the

TABLE 4

ABLATION TEST CONDITIONS

Test No.	Material	$T_{-\infty}$ Initial Mat. Temp.--°F	T_∞ Air Temp. °F	$\bar{U}_\infty$ Air Velocity ft/sec	Re_g Air Reynolds No. (X 10^4)	Pr_g Air Prandtl No.
26	650 Oil	-30	72	35.0	7.56	0.712
27	650 Oil	-30	72	50.0	10.81	0.712
28	650 Oil	-30	72	75.0	16.22	0.712
29	650 Oil	-30	150	35.0	5.99	0.708
30	650 Oil	-30	150	50.0	8.56	0.708
31	650 Oil	-30	150	75.0	12.81	0.708
32	Glycerol	-30	72	33.4	7.22	0.712
33	Glycerol	-30	72	50.0	10.81	0.712
34	Glycerol	-30	72	75.0	16.22	0.712
35	K-312 Resin	-30	68	32.8	7.15	0.713
36	K-312 Resin	-30	72	50.0	10.81	0.712
37	K-312 Resin	-30	150	35.0	5.99	0.708
38	K-312 Resin	-30	150	50.0	8.56	0.708
39	K-312 Resin	-30	150	75.0	12.81	0.708
40	K-312 Resin	-30	168	50.8	8.24	0.708
41	K-312 Resin	-30	120	50.0	9.20	0.710
42	K-312 Resin	-30	150	40.0	6.85	0.708
43	Pen 50 Asph.	-30	150	75.0	12.81	0.708
44	Pen 50 Asph.	---	---	---	---	---
45	Pen 50 Asph.	-30	150	50.0	8.56	0.708
46	Pen 50 Asph.	-30	168	50.0	8.10	0.708
47	20 W Oil	-30	72	75.0	16.22	0.712
48	20 W Oil	-30	72	50.0	10.81	0.712
49	20 W Oil	-30	72	40.0	8.64	0.712
50	20 W Oil	-30	72	35.0	7.56	0.712
51	20 W Oil	-30	120	35.0	6.44	0.710
52	20 W Oil	-30	150	35.0	5.99	0.708
53	20 W Oil	-30	178	35.0	5.44	0.707
54	Paraffin	---	---	---	---	---
55	20 W Oil	-30	132	50.0	7.30	0.709
56	20 W Oil	-30	150	50.0	7.13	0.708
57	20 W Oil	-30	176	52.0	7.06	0.707

surface of the paraffin sample, but they could not be photographed or measured with the available equipment.

Test number 44 was performed to verify the critical Reynolds number for the pen 50 asphalt. No wave information was recorded.

Test number 35 served as one limiting case of the parameter γ ($\gamma = 0$) since the air stream temperature was exactly equal to the sample softening temperature. (See Table 5.) Although test number 36 has a value of γ which is not actually 0, the value is so close to 0 that the data is essentially similar to test 35. The largest value of γ ($\gamma = 1.97$) was obtained in test 53 in which oil softening at $-30^{\circ}F$ was ablated in an air stream at $176^{\circ}F$, which was the limit of the heater capacity at an air velocity of 52 feet per second. The smallest measurable, non-vanishing value of γ was 0.01, obtained in tests 43 and 45. Thus, the tests covered a range of two orders of magnitude in the parameter γ including values of unit order.

The measurements of wave velocity and spacing were taken from the 16mm. films. Waves were measured on the back half of the plate away from the leading edge of the material. During the testing it was noted that individual waves did not move at constant velocity but accelerated and decelerated at random. It was not unusual for a wave to slow nearly to a stop and then

TABLE 5

ABLATION TEST RESULTS

Test No.	Wave Data			Wave Parameter	Surface Temp.	
	Wave Velocity, $\bar{U}_w$ ft/sec X 10^3	Wave Amplitude, $\bar{Y}_w$ ft X 10^{-3}	Wave Length $\bar{L}_w$ ft X 10^{-2}	γ	Ti-Calculated °F	Ti-Measured °F
26	18.5	9.76	28.6	0.31	56.3	54
27	26.2	7.10	22.7	0.31	56.3	63
28	39.2	5.16	8.98	0.31	56.3	61
29	67.9	0.83	11.9	1.14	71.6	70
30	97.1	6.41	13.5	1.14	71.6	71
31	155.0	4.41	12.3	1.14	71.6	71
32	8.74	18.80	15.6	0.64	33.5	30
33	70.0	12.00	16.5	0.64	33.5	--
34	100.0	9.68	15.5	0.64	33.5	--
35	0.0	---	---	0.00	68.0	59
36	0.09	10.00	---	≈0	71.9	60
37	9.10	1.67	7.95	0.26	128.3	123
38	19.7	8.00	18.1	0.26	128.3	129
39	29.2	5.66	10.7	0.26	128.3	128
40	29.7	5.58	11.2	0.38	133.9	134
41	5.91	9.83	15.3	0.10	113.2	105
42	15.9	9.34	33.8	0.26	128.3	129
43	1.13	14.15	19.8	0.01	149.8	138
45	0.62	13.40	20.4	0.01	149.8	137
46	3.56	12.90	28.6	0.69	150.0	146
47	155.0	6.66	12.8	0.89	24.1	--
48	109.0	9.16	14.4	0.89	24.1	20
49	88.4	8.33	15.3	0.89	24.1	27
50	84.5	7.16	20.1	0.89	24.1	20
51	123.0	5.50	16.1	1.38	33.0	33
52	131.0	5.66	10.3	1.70	36.8	--
53	155.0	5.00	14.9	1.97	40.0	--
55	194.0	6.66	12.7	1.51	34.5	--
56	207.0	6.17	11.7	1.70	36.8	--
57	220.0	5.83	12.5	1.95	39.8	--

move rapidly for a distance. This same fact was noted during measurement of wave characteristics, and it was found to be necessary to take an average of several values to obtain consistent results. Individual values were found to vary by as much as 30% to 40% even after steady melting had begun. The wave data listed in Table 5 represents an average of 4 or more values for each measured quantity. The amplitude and wave length measurements for test 46 proved to be completely unreasonable and do not fit the patterns established by the other tests. No explanation has been found for this large discrepancy, and it is assumed that test 46 is faulty for some unknown reason.

Certain patterns can be discerned from the data in dimensional form; however more meaningful conclusions can be seen by non-dimensionalizing the various quantities, and this latter approach will be used here.

Analysis of results

The general approach to a complex flow situation would involve the principles of dimensional analysis and similitude in an attempt to find scale factors and dimensionless ratios which can be used to reduce the various combinations of variables to more convenient form. Fortunately, the work of Chen (26) and Ostrach (25) has provided possible ratios based on analysis of

the basic equations.

Of the parameters provided by Chen (Appendix), the ablation parameter, γ; the reference velocity, $\bar{U}r$; the liquid boundary layer thickness, δ_1; and the interface temperature, Ti, are found to be useful in the present problem.

The first step in utilizing these parameters involves calculating Ti from equations A and B (Appendix) and the viscosity-temperature profile. Chen suggests that the reference temperature, To, may be taken as being equal to Ti without loss of generality. The advantage of doing so is that the power law for the liquid viscosity, $\mu_i = \mu_o (Ti/To)^{-N}$, becomes trivial and is not needed. In the event that the viscosity deviates from such a law, accuracy is improved by using the actual viscosity-temperature relation rather than the power law assumption. The disadvantage is that μ_o in equation A is now μ_i, which varies with Ti, the unknown in the calculation. The solution for Ti must be obtained by trial-and-error solution of the relation

$$\left[\frac{(T_\infty - Ti)^3}{(Ti - T_{-\infty})(Ti - Tm)^2}\right]^{\frac{1}{3}} = \left[\frac{k_l^2 c_{pl} \rho_l \mu_g}{k_g^2 c_{pg} \rho_g \mu_i}\right] \frac{1}{(Pr_g)^{(3m-1)}} \qquad \text{-------(1)}$$

for which the actual temperature-viscosity profile is needed to identify μ_i for each trial value of Ti. After Ti has been obtained, γ and the remaining parameters can

immediately be calculated.

Tables 5 and 6 contain the values of the calculated parameters and the non-dimensionalized results for the present tests. In some cases it was also possible to obtain measurements of the actual interface temperature from the thermocouple records of the tests, and these values are listed in the last column of Table 5. By plotting the readings of thermocouples near the melting surface against time, the moment at which the junction broke through the surface could be identified from the resulting sudden change in slope. The results listed should be regarded as correct only to the order of magnitude, because the exact values cannot be well distinguished by this method; in fact, the results from several tests were inconclusive and were omitted from the tabulation. Nevertheless, there is a correlation between the measured and the calculated values as can be seen by comparing the last two columns in Table 5.

The nature of the parameter γ can be examined from equation B (Appendix).

$$\frac{(T_\infty - T_i)^3}{(T_i - T_\infty)(T_i - T_m)^2} = \gamma^3 \qquad \text{----------(2)}$$

The numerator of this ratio governs the slope of the temperature profile in the gas stream at the interface; therefore it governs the rate at which heat is supplied to the interface. The first term in the denominator

TABLE 6

PARAMETERS AND NON-DIMENSIONALIZED RESULTS

Test Number	Velocity		Amplitude		Wave Spacing		
	Ref. Velocity-$\bar{U}_r$ ft/sec X 10^{-3}	Dimensionless Velocity-$\bar{U}_w/\bar{U}_r$	Liquid B. L. Thickness @ 10 in. (X 10^{-3})	$\frac{\bar{Y}_w}{\delta_l}$ @ x = 10 in. L_x	x Value Where L_w Was Measured	Liquid B. L. Thickness (X 10^{-3})	Dimensionless Spacing- $\frac{L_w}{\delta_l} L_x$
26	2.65	6.99	98.6	.099	.840	97.9	3.49
27	3.80	6.90	82.5	.086	.972	76.3	3.07
28	5.70	6.80	67.2	.077	1.045	60.0	1.43
29	2.66	25.5	27.4	.030	.733	29.2	5.26
30	3.80	25.6	22.8	.280	1.001	20.8	6.42
31	5.70	26.2	18.8	.235	1.055	16.6	6.99
32	0.62	14.1	83.7	.225	.514	106.	2.85
33	0.92	33.1	68.4	.175	.940	64.3	2.71
34	1.39	30.0	55.9	.173	.980	51.5	3.07
35	0.00	0.00	---	---	---	---	---
36	≈0	≈0	1110.	.009	---	---	----
37	2.22	4.10	95.6	.017	.501	123.	1.27
38	3.17	6.20	80.0	.100	.989	73.9	2.50
39	4.76	6.13	65.4	.086	1.020	59.0	1.78
40	3.34	8.89	55.3	.100	1.040	49.5	2.20
41	2.66	2.23	192.	.051	.996	176.	0.87
42	2.53	6.28	89.6	.104	.965	84.8	4.21
43	3.05	0.37	996.	.014	1.016	90.1	0.21
45	2.03	0.30	1220.	.011	.951	1140.	0.19
46	0.23	15.5	14.0	.920	.988	12.8	22.60
47	6.90	22.4	27.5	.242	1.028	24.7	5.03
48	4.60	23.7	33.7	.272	.940	31.7	4.83
49	3.68	23.9	37.7	.221	.952	35.2	4.57
50	3.22	26.2	40.4	.178	.972	37.3	5.52
51	3.22	38.1	25.0	.219	.895	24.1	7.45
52	3.17	41.3	21.3	.266	.776	22.0	6.07
53	3.04	51.0	18.5	.270	.883	18.0	9.39
55	4.58	42.3	18.4	.301	.974	20.4	6.39
56	4.53	45.8	19.4	.318	1.005	17.6	6.61
57	4.56	48.3	16.5	.354	.957	15.3	8.55

establishes the rate at which heat is conducted into the interior of the body, while the second term establishes the rate at which material is melting. The ratio, then, is the relation between the incident heating rate and the combined heating and softening rates of the ablating body. Large γ values are associated with materials which heat and melt slowly in high-temperature air streams.

It should be noted from equation (1) that the interface temperature is dependent upon the material properties; therefore the significance of γ is also tied to the material properties but not so clearly. Equation A from the Appendix provides the appropriate relationship, which becomes

$$\gamma = \left[\frac{k_l^2 c_{pl} \rho_l \mu_g}{k_g^2 c_{pg} \rho_g \mu_i}\right] \frac{1}{(Pr_g)^{(3m-1)}} \qquad \text{----------(3)}$$

Cursory examination of this equation seems to indicate that increasing γ values would be associated with increasing liquid thermal conductivities and specific heats and therefore with increasing rates of heat gain by the melting body. This statement is contradictory to the conclusion drawn from equation (2), which indicates that large γ values are associated with small rates of body heating and softening. The answer to the apparent contradiction lies in the fact that μ_i

appears in the denominator of equation (3). Large thermal conductivities and specific heats in the ablating body will tend to keep the interface temperature, Ti, low; and since μ_i varies rapidly as some inverse power of Ti, the rate of increase of μ_i will be greater than the rate of increase of k_l or c_{pl}. Hence large γ is associated with small body heating and melting rates as deduced from equation (2).

After some experimentation it was found that striking trends could be revealed by non-dimensionalizing the wave velocity with respect to the reference velocity, $\bar{U}r$, and the wave amplitude and spacing with respect to the liquid boundary layer thickness, δ_l. These scaled values are also listed in Table 6.

The non-dimensionalized wave velocity was then plotted against the ablation parameter, γ, with the result being a straight line passing through the origin, which can be approximately represented by the equation $\bar{U}w/\bar{U}r = 25\gamma$ (figure 15). The agreement of data points with this line is rather good except for tests numbered 33 and 34 (circles around points in figure 15). These two were tests using glycerol in which accidental contamination of the specimen was suspected. The excessively high wave velocity here seems to agree with the lowering of viscosity that would occur with the addition of isopropyl alcohol to the glycerol.

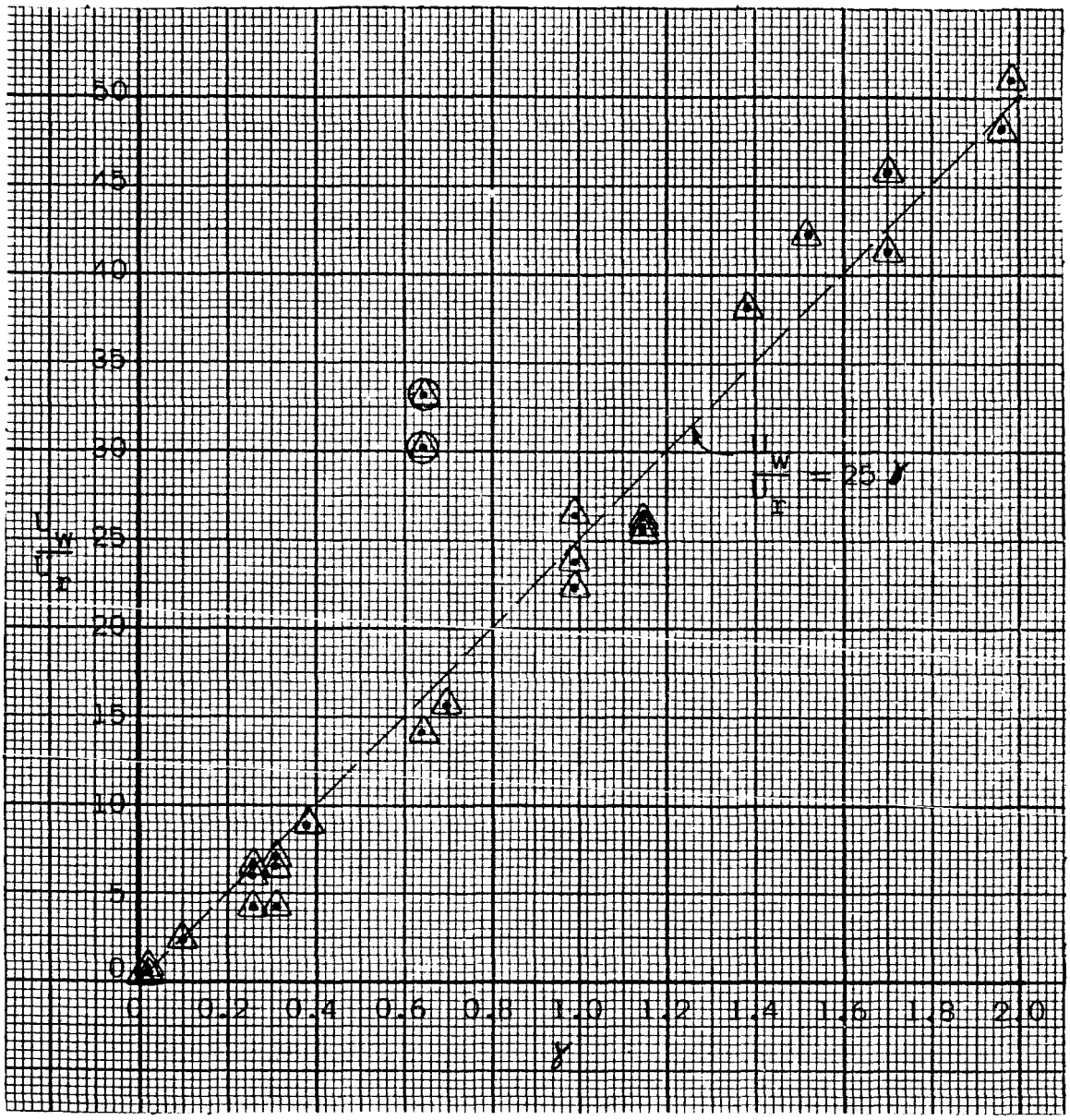

Figure 15--Plot of Non-Dimensional Wave Velocity Versus Ablation Parameter γ.

From the equation of this line it can be seen that $\bar{U}w = 25\bar{U}r\gamma$. If the values of $\bar{U}r$ and γ from the appendix are substituted, the result is

$$\bar{U}w = 25\bar{U}r\gamma = 25\bar{U}_{\infty}\left[\frac{Ti - Tm}{Ti - T_{-\infty}}\right]^{\frac{1}{3}} \left[\frac{c_{pl}(Pr_g)^{(1-m)}}{c_{pg}(Pr_l)}\right] \qquad \text{-------(4)}$$

The quantities in the first bracket essentially define the ratio between the rate of melting and the rate at which heat is transmitted to the interior of the body. Large wave velocities will result when the air stream velocity is large or if the initial body temperature is of the same order as the softening temperature. Although the term in the first bracket is less than one ($Tm > T_{-\infty}$) and approaches unity asymptotically as Ti is increased, the velocity will continue to increase with increasing Ti since the liquid viscosity, μ_i (in Pr_l), decreases rapidly with increasing Ti. The result is a steadily increasing wave velocity as Ti and γ increase.

The wave velocity depends on the material specific heat, not because of equation (4) where it appears in both numerator and denominator, but from equation (1). Increasing c_{pl} causes Ti to decrease thereby decreasing $\bar{U}w$. This effect is stronger at low γ values when the first bracket in equation (4) is most effective.

In a similar way an increase of thermal

conductivity, k_1, will cause Ti to decrease; however k_1 appears in the numerator of equation (4) which tends to cancel the effect of lowering Ti. When Ti is large compared to Tm and $T_{-\infty}$, the effect on the first bracket is small, and increasing k_1 will cause $\bar{U}w$ to increase. At low γ values it is possible that the reverse could be true.

The wave amplitudes were scaled with respect to the dimensional liquid boundary layer thickness, $\delta_1 L_x$, where δ_1 is the non-dimensional thickness (equation F, Appendix) and L_x is the dimensional distance from the plate leading edge to the point at which the amplitude was measured (10 inches). The value of δ_1 was calculated using the gas Reynolds number based on the same distance from the plate leading edge. The results are in Table 6, and figure 16 contains the scaled amplitudes plotted against γ with the exception of the tests which were taken very near the critical air velocity. These last are omitted since the waves appeared and disappeared at intervals and frequently were not in range of the amplitude probe. Although spacing and velocity information could be obtained from the films, the erratic behavior of the waves near the critical point prevented effective measurement of amplitude. As can be seen in figure 16, the relationship between the non-dimensional amplitude and γ is not linear

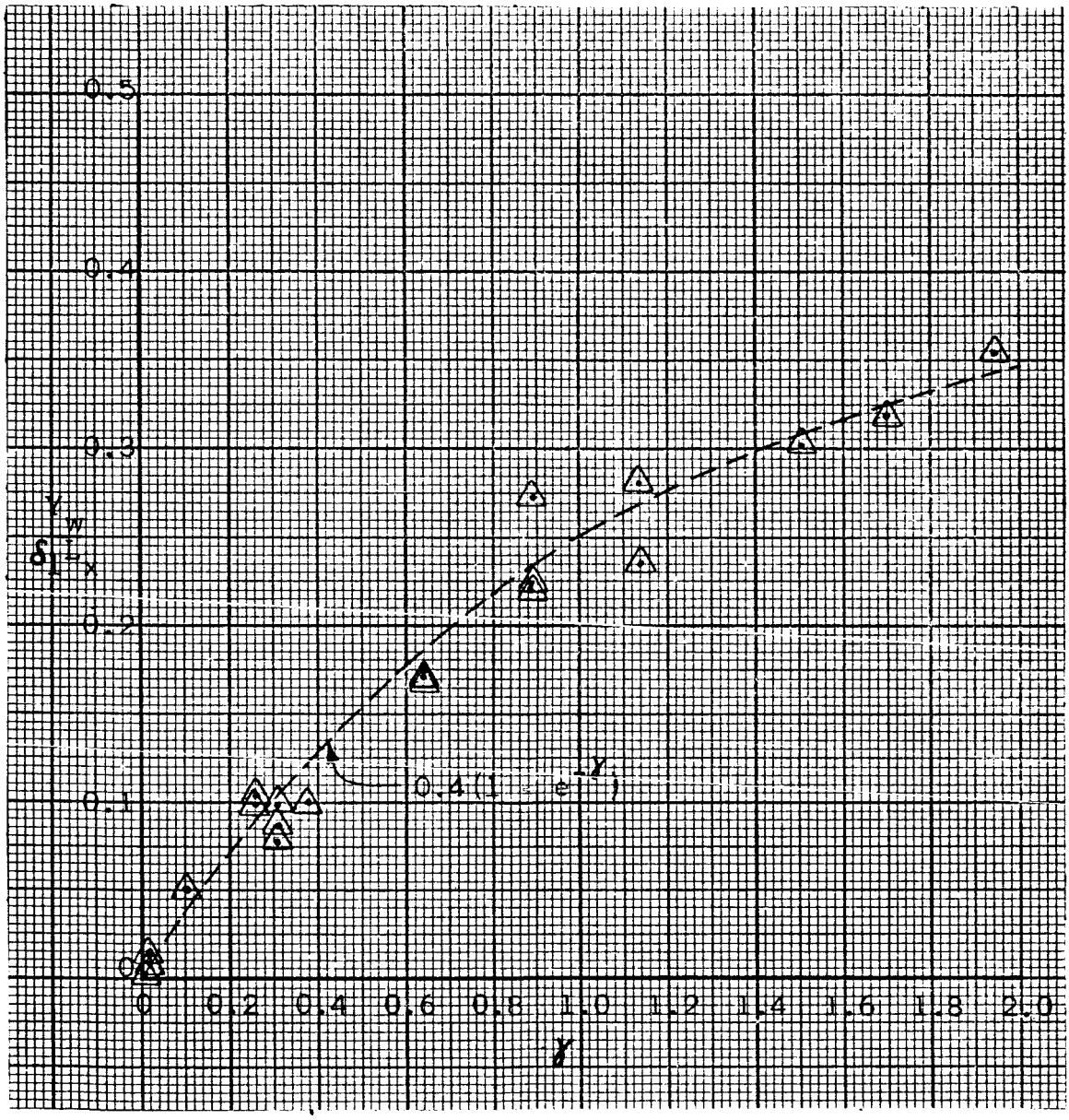

Figure 16--Plot of Non-Dimensional Wave Amplitude Versus Ablation Parameter γ.

but rather tends to become more constant at higher values of γ. Considering that $\overline{Y}w/\delta_1 L_x$ represents the ratio between the wave amplitude and the liquid boundary layer thickness (i.e., film thickness), it is reasonable that this ratio will not continue to increase indefinitely. The wave can be expected to occupy some fraction of the film layer (here about 1/3 when $\gamma = 2$) with a maximum value less than unity. This possibility is supported by the fact that the data can be rather well represented by the asymptotic relation

$$\frac{\overline{Y}w}{\delta_1 L_x} = 0.4(1 - e^{-\gamma}) \qquad \text{----------(5)}$$

which is shown as a dotted line in figure 16.

This equation is only meant to represent the data as it stands. Complete verification of the relation would depend on more amplitude measurements in the range above $\gamma = 2$ to see whether or not the ratio would actually approach 0.4 as predicted by equation (5).

The behavior of the wave amplitude can be examined by writing equation (5) in complete form.

$$\overline{Y}w = 0.4\left[\frac{Ti - Tm}{T\infty - Ti}\right]\left[\frac{k_l}{k_g (Pr_g)^m (Re_g)^{1/2}}\right](1 - e^{-\gamma}) \qquad \text{-------(6)}$$

For large values of γ equation (6) becomes approximately

$$\overline{Y}w = 0.4\left[\frac{Ti - Tm}{T\infty - Ti}\right]\left[\frac{k_l}{k_g (Pr_g)^m (Re_g)^{1/2}}\right](1 - e^{-\gamma}) \qquad \text{--------(7)}$$

Obviously, $\bar{Y}w$ decreases in proportion to $(Re_g)^{1/2}$ which is in general agreement with the present data. As the heating rate becomes large (large γ), the amplitude decreases asymptotically to zero because of the fact that the first bracket in equation (7) is essentially like the reciprocal of γ.

The effect of increasing k_1 is not immediately obvious since Ti is coupled to k_1 as before. From examination of equations A and B in the Appendix, it can be seen that the first factor in equation (7) decreases in proportion to k_1^2; and this fact combined with the k_1 in the numerator of the second factor points to a decrease in $\bar{Y}w$ proportional to k_1^{-1}.

The wave lengths or spacings, $\bar{L}w$, were non-dimensionalized with respect to the dimensional boundary layer or film thickness, $\delta_1 L_x$, at the point where the lengths were measured. Normally this point was approximately 1 foot behind the plate leading edge; however several measurements were taken at other points when the air speed was near the critical value and waves did not cover the entire surface. The scale factors and the non-dimensionalized results are listed in Table 6.

Plotting the scaled wave spacings against γ results in a definite pattern although with a rather large amount of scatter (figure 17). The reason for the scatter is not clear except for the fact that the

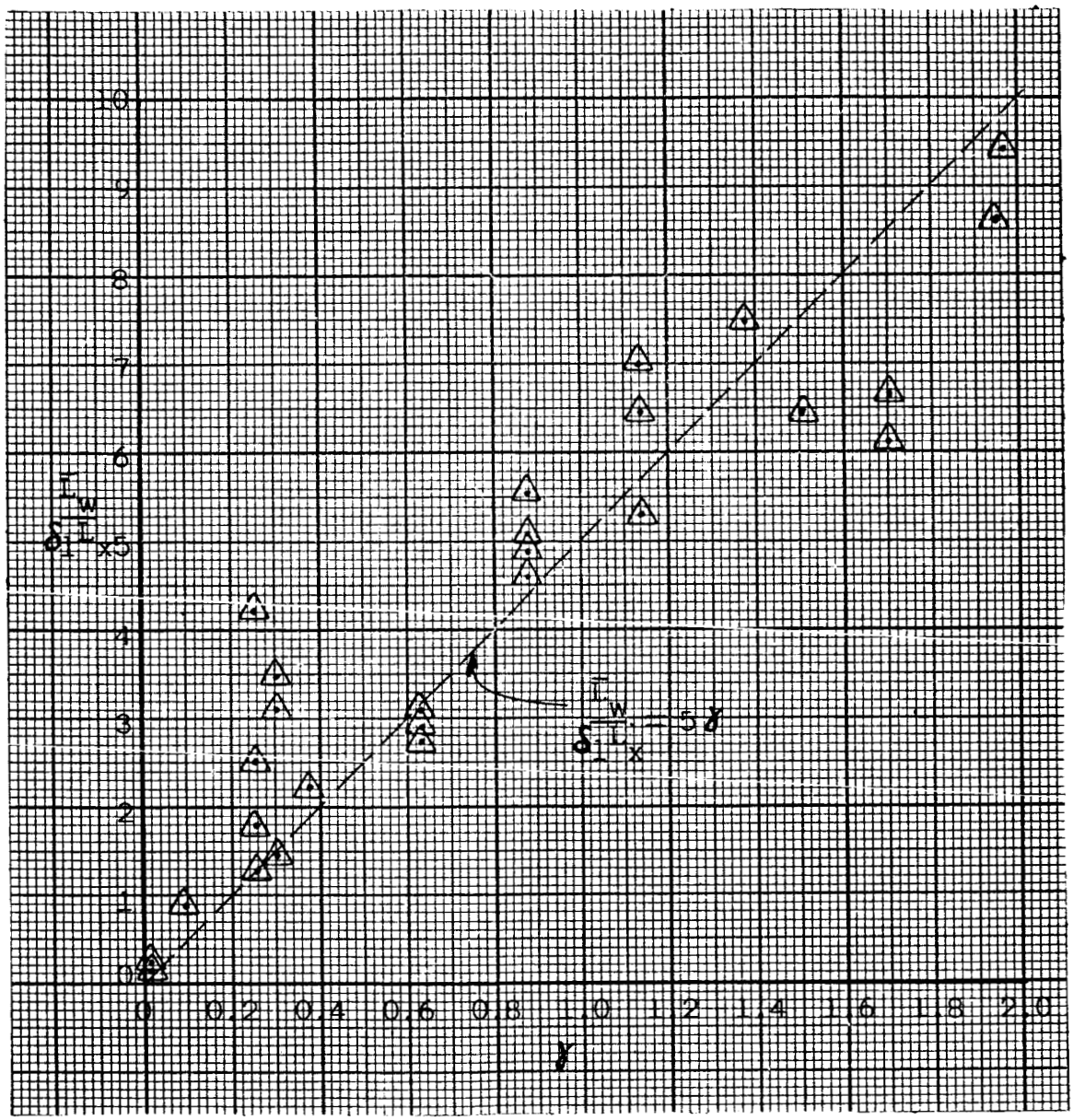

Figure 17--Plot of Non-Dimensional Wave Spacing Versus Ablation Parameter γ.

spacing was the most erratic and variable quantity measured.

The pattern, however coarse it may be, can be conveniently approximated by the equation

$$\frac{\bar{L}w}{\delta_1 L_x} = 5\gamma \qquad \text{----------(8)}$$

Obviously the wave length increases in proportion to either γ or the film thickness, δ_1; however γ and δ_1 are not independent of one another, and the effects must be investigated from the product of the two factors. That is,

$$\bar{L}w = 5L_x\left[\frac{\bar{T}i - \bar{T}m}{\bar{T}i - T_\infty}\right]^{\frac{1}{3}}\left[\frac{k_1}{k_g(Pr_g)^m(Re_g)^{1/2}}\right] \qquad \text{---------(9)}$$

Since the value of the first bracket is less than unity and increases toward unity as Ti increases, it follows that the wavelength at a given point on the plate should increase as Ti increases. Equation (9) also indicates that $\bar{L}w$ decreases in proportion to $(Re_g)^{1/2}$ but increases in proportion to the square root of the distance along the plate. The latter conclusion is true since L_x appears also within the Reynolds number.

Again, the effects of varying the material properties cannot be seen without considering that Ti is a function of those properties through equations A and B in the Appendix. With everything else held constant, an increase in k_1 causes a decrease in Ti and a net

increase in wavelength if the first factor in equation (9) is of unit order. If this factor is smaller, the effect of k_1 is not clear since the rate of variation of this factor with respect to k_1 is not readily determined.

Relationship to the original problem

The results in the present study are directly applicable only to the particular configuration and conditions used for the tests. Direct application of the information obtained here to other configurations must be done with care and consideration of the effects of changing shapes. The important point is that the analysis and parameters proposed by Chen are quite useful in the examination of melting wave behavior. Using this information, it is possible to predict melting wave behavior from knowledge of the material properties and the ambient conditions. Since Chen's analysis is not restricted to the flat plate case, it should be possible to apply his results to other configurations in a manner similar to that used in this study.

The behavior of melting waves is of interest in the tektite problem discussed earlier. Using the temperature-viscosity curves for tektite glass in reference 12, it is possible to estimate the value of δ for this material in an air stream at high temperatures.

Assuming a Tm of 1200°K and a T_∞ of 4000°K, it appears that the value of γ would be of the order of unity, which is within the range of the present tests.

To expand and continue the work described herein, several avenues could be investigated. The most important questions remaining are related to the effects of body shape, deceleration forces, and pressure gradients upon the waves encountered here.

The most serious limitation encountered in the present tests was the relative inaccuracy of available information about the physical properties of the melting materials. Now that basic patterns have been established, refinement would be possible by obtaining accurate measurements of properties for one or two materials and then using these for a series of tests. During this project several materials were used to insure against developing results which would be peculiar to a particular type. It has been verified that the effects of material properties can be incorporated mathematically via the parameters and scale factors proposed by Chen; hence a variety of materials is no longer needed.

To extend and improve the results discussed here for the flat plate, higher values of γ should be studied, the effects of turbulence should be considered, and the behavior of the so-called critical point should be examined in detail.

Summary

The experiments described in this report have provided the following information:

1. A study of the minimum conditions required to generate waves on melting materials.
2. Specific data covering melting waves over a range of conditions.

As a result of this project several facts concerning melting wave behavior have been established or verified. In agreement with results from some earlier works, the existence of at least two different types or modes of wave behavior have been shown to exist; and the basic conditions for the formation of each type have been at least partly determined. Furthermore, it appears that the second type--the one depending largely on the gas stream Reynolds number for its formation--is the one which corresponds to the type seen in melting materials.

Utilizing the parameters developed by Chen (26) and predicted earlier by Ostrach and McConnell (25), definite mathematical relationships have been developed between the wave characteristics (velocity, amplitude, and spacing); the material properties; the gas stream properties; and the ambient conditions existing during melting. Since the properties and conditions are known or can be determined, it is thus possible to predict the wave characteristics from the appropriate relations.

Some correlation has been shown between the results of these tests and the theories concerning stability analyses of liquid film layers. In addition, it has been shown that the present tests likely are representative of tektite ablation.

APPENDIX

RESULTS FROM CHEN'S ANALYSIS

The following quantities are shown by Chen to be significant in melting wave behavior:

1. Ablation parameter, γ.

$$\gamma \triangleq \left[\frac{k_l^2 c_{pl} \rho_l \mu_g}{k_g^2 c_{pg} \rho_g \mu_o}\right] \frac{1}{(Pr_g)^{(3m-1)}} \qquad \text{-------(A)}$$

where: $m = 1$ if $Pr_g > 1$
$m = \frac{1}{2}$ if $Pr_g < 1$

2. Interface temperature, Ti.

$$\left[\frac{(T\infty - Ti)^3}{(Ti - T_{-\infty})(Ti - Tm)^2}\left(\frac{To}{Ti}\right)^n\right] \triangleq \gamma^3 \qquad \text{-------(B)}$$

note: To can be set equal to Ti without loss of generality.

3. Reference velocity, $\bar{U}r$.

$$\bar{U}r \triangleq \bar{U}_\infty \left[\frac{c_{pl}(Pr_g)^{(1-m)}}{c_{pg} Pr_l}\right]\left[\frac{Ti - Tm}{T\infty - Ti}\right] \qquad \text{-------(C)}$$

4. Reference time, σ.

$$\sigma \triangleq \left[\frac{L_x Pr_l c_{pg}}{\bar{U}_\infty (Pr_g)^{(1-m)} c_{pl}}\right]\left[\frac{Ti - T\infty}{Tm - Ti}\right] \qquad \text{-------(D)}$$

5. Gas boundary layer thickness, δ_g.

$$\delta_g \triangleq \frac{1}{(Re_g)^{1/2}} \qquad \text{----------(E)}$$

6. Liquid boundary layer (or film) thickness, δ_l.

$$\delta_l \triangleq \left[\frac{-k_l}{k_g (Pr_g)^m (Re_g)^{1/2}}\right]\left[\frac{Ti - Tm}{T\infty - Ti}\right] \quad \text{-------(F)}$$

7. Gas temperature layer thickness, e_g.

$$e_g \triangleq \frac{1}{(Pr_g)^m (Re_g)^{1/2}} \quad \text{----------(G)}$$

8. Liquid temperature layer thickness, e_l.

$$e_l \triangleq \left[\frac{-k_l}{k_g (Pr_g)^m (Re_g)^{1/2}}\right]\left[\frac{Ti - T_{-\infty}}{T\infty - Ti}\right] \quad \text{------(H)}$$

SUMMERY OF DERIVATION OF ABLATION PARAMETERS

Since Chen's work (26) has not been completed at the time of this writing, the essential features of the development of the ablation parameters are summarized here. Eventually the complete work will appear in Chen's thesis, which will be available through the library at Case Institute of Technology.

The mathematical model was developed under the following assumptions:

1. The viscosity-temperature profile of the material is assumed to be of the form $\mu/\mu_o = (T/T_o)^{-n}$.
2. Density, specific heat, and thermal conductivity are assumed to be constant.
3. The evaporation of the liquid from the gas-liquid interface is assumed to be negligible.
4. The body may be subjected to constant deceleration or acceleration.
5. The gas velocity is assumed to be much greater than the interfacial velocity.
6. The ablation wave amplitude is small compared to the wave length.
7. The liquid layer is assumed to be small compared to the characteristic body length.

A coordinate system is fixed to the body in such a way that X is the distance measured along the original body surface from the stagnation point (or from the

leading edge of a sharp body) and Y is measured along the local normal to the surface. The equations of motion then become for the liquid

Continuity:

$$\frac{\partial}{\partial X}(R^{\epsilon}\bar{U}) + \frac{\partial}{\partial Y}(R^{\epsilon}\bar{V}) = 0 \qquad \text{----------(a)}$$

Where $\epsilon = 0$ for two-dimensional bodies and $\epsilon = 1$ for axisymmetric bodies.

Momentum:

$$\rho\left[\frac{\partial \bar{U}}{\partial \bar{t}} + \bar{U}\frac{\partial \bar{U}}{\partial X} + \bar{V}\frac{\partial \bar{U}}{\partial Y} - \sqrt{1 - \left(\frac{dR}{dX}\right)^2}\,A\right] = -\frac{\partial P}{\partial X} + \frac{\partial}{\partial Y}\left[\mu\left(\frac{\partial \bar{V}}{\partial X} + \frac{\partial \bar{U}}{\partial Y}\right)\right] + 2\frac{\partial}{\partial X}\left[\mu\frac{\partial \bar{U}}{\partial X}\right] \text{---(b)}$$

$$\rho\left[\frac{\partial \bar{V}}{\partial \bar{t}} + \bar{U}\frac{\partial \bar{V}}{\partial X} + \bar{V}\frac{\partial \bar{V}}{\partial Y} - \frac{dR}{dX}A\right] = -\frac{\partial P}{\partial Y} + \frac{\partial}{\partial X}\left[\mu\left(\frac{\partial \bar{U}}{\partial Y} + \frac{\partial \bar{V}}{\partial X}\right)\right] + 2\frac{\partial}{\partial Y}\left[\mu\frac{\partial \bar{V}}{\partial Y}\right] \text{---(c)}$$

Energy: (Neglecting thermal expansion of the liquid)

$$\rho c_p\left[\frac{\partial \bar{T}}{\partial \bar{t}} + \bar{U}\frac{\partial \bar{T}}{\partial X} + \bar{V}\frac{\partial \bar{T}}{\partial Y}\right] = k\left[\frac{\partial^2 \bar{T}}{\partial X^2} + \frac{\partial^2 \bar{T}}{\partial Y^2}\right] + \Phi \qquad \text{---------(d)}$$

where $$\Phi = \mu\left[2\left(\frac{\partial \bar{U}}{\partial X}\right)^2 + 2\left(\frac{\partial \bar{V}}{\partial Y}\right)^2 + 2\frac{\partial \bar{U}}{\partial Y}\frac{\partial \bar{V}}{\partial X} + \left(\frac{\partial \bar{U}}{\partial Y}\right)^2 + \left(\frac{\partial \bar{V}}{\partial X}\right)^2\right] \qquad \text{---------(e)}$$

Interface: (I.e., $Y = H(X,\bar{t})$

$$\frac{\partial H}{\partial \bar{t}} + \bar{U}_i\frac{\partial H}{\partial X} - \bar{V}_i = 0 \qquad \text{----------(f)}$$

These equations are non-dimensionalized using the following relations:

$$u = \frac{\bar{U}}{Ur} \; ; \quad v = \frac{\bar{V}}{Ur\delta_1} \; ; \quad p = \frac{P}{Po} \; ; \quad \Theta = \frac{T - Tm}{Ti - T_{-\infty}} \; ;$$

$$r' = \frac{R}{L} \; ; \quad x = \frac{X}{L} \; ; \quad y = \frac{Y}{L\delta_1} \; ; \quad \underline{Y} = \frac{Y}{Le_1} = y\frac{\delta_1}{e_1} \; ;$$

$$t = \frac{\bar{t}}{\sigma} \; ; \quad \eta = \frac{H}{L\delta_1} \; ; \quad g = \frac{AL\rho_1}{P_o} \; ; \quad \mu = \frac{\bar{\mu}}{\mu_i}$$

where $\bar{U}r, \mu_i, Ti, P_o, L, \delta_1, e_1$ are reference quantities. The resulting forms are as follows:

$$u_x + v_y = 0 \qquad \text{----------(g)}$$

$$\left[\frac{L}{\sigma Ur}\right]u_t + uu_x + vu_y - \left[\frac{P_o}{\rho_1 U_r^2}\right](\sqrt{1 - r'^2}\; g - p_x) = \left[\frac{\mu_i}{\rho_1 LUr\delta_1^2}\right]\frac{\partial}{\partial y}(\delta_1^2 v_x + u_y) + 2\delta_1^2\frac{\partial}{\partial x}(uu_x) \quad \text{----(h)}$$

$$\left[\frac{L}{\sigma U_r}\right]v_t + uv_x + vv_y - \left[\frac{P_o}{\rho_1 U_r^2 \delta_1^2}\right](\delta_1 gr' - p_y) = \left[\frac{\mu_i}{\rho_1 LU_r \delta_1^2}\right]\left[\frac{\partial}{\partial x}(u\delta^2 v_x + uu_y) + 2\frac{\partial}{\partial y}(uv_y)\right] \quad \text{---(i)}$$

$$\left[\frac{L}{\sigma U_r}\right]\Theta_t + u\Theta_x + \left[\frac{\delta_1}{e_1}\right]v\Theta_y = \left[\frac{k}{c_p\rho_1 LU_r e_1^2}\right](e_1^2\Theta_{xx} + \Theta_{yy}) + \left[\frac{\mu_{iUr}}{(Ti - T_{-\infty})Lc_p\rho_1\delta_1}\right]\Phi \quad \text{-(j)}$$

where $\Phi = \mu_i\left[\delta_1^2(2u_x^2 + 2v_y^2 + 2u_y v_x) + (u_y^2 + \delta_1^4 v_x^2)\right]$ -(k)

$$\left[\frac{L}{\sigma U_r}\right]\eta_t + u_{(i)}\eta_x - v_{(i)} = 0 \qquad \text{----------(l)}$$

The appropriate boundary conditions may be established in non-dimensional form as:

at $y = \eta(x,t)$

$$Q_i = fct(x,t)(T_\infty - Ti) = -\left[\frac{k_g(T_\infty - Ti)}{Le_g}\right]\frac{\partial \theta_g}{\partial y}\Big|_i = -\left[\frac{k_l(Ti - T_{-\infty})}{Le_l}\right]\frac{\partial \theta_l}{\partial y}\Big|_i \quad \text{--(m)}$$

$$T_{gi} = T_{li} \quad \text{----------(n)}$$

$$Ti_g(x,t) = \left[\frac{\mu_g \bar{U}_\infty}{L\delta_g}\right]\frac{\partial u_g}{\partial y}\Big|_i = \left[\frac{\mu_i \bar{U}_r}{L\delta_l}\right]\frac{\partial u_l}{\partial y}\Big|_i \quad \text{---(o)}$$

for $y \rightarrow -\infty$

$$T \rightarrow Tm \qquad \therefore \theta \rightarrow 0 \quad \text{----------(p)}$$

$$u \rightarrow 0 \quad \text{----------(q)}$$

$$v \rightarrow v_{-\infty} \quad \text{----------(r)}$$

at $x = 0$

$$\frac{\partial \eta}{\partial x} = 0, \quad \eta = 0 \quad \text{----------(s)}$$

$$\frac{\partial \theta}{\partial x} = \frac{\partial u}{\partial x} = \frac{\partial v}{\partial x} = 0 \quad \text{----------(t)}$$

and

$$\frac{\bar{\mu}}{\mu_o} = \left(\frac{T}{To}\right)^{-N} \quad \text{----------(u)}$$

For a particular problem the following terms would be known: $T_{-\infty}$, T_∞, $\bar{U}_\infty$, L, ρ_l, ρ_g, μ_g, Tm, N, k, c_p. However, the reference quantities, Ti, $\bar{U}r$, σ, μ_i, δ_l,

e_1, δ_g, e_g, and P_o are not directly available but must be obtained from an order-of-magnitude analysis of the non-dimensionalized equations. Chen offers the following reasoning:

A. P_o may arbitrarily be taken as being equal to the largest pressure in the flow region (i.e., the stagnation pressure).

$$P_o \triangleq \bar{U}^2 \rho_g \qquad \text{----------(a')}$$

B. Based on assumption (5), the order of magnitude of the boundary and thermal layers may be taken as

$$\delta_g \triangleq \frac{1}{(Re_g)^{1/2}} ; \qquad \text{----------(b')}$$

$$e_g \triangleq \frac{1}{(Re_g)^{1/2} Pr_g{}^m} \qquad \text{----------(c')}$$

where: $m = 1$ when $Pr_g > 1$

$m = \frac{1}{2}$ when $Pr_g < 1$

C. The quantity μ_i may be obtained from equation (u) if Ti is known. That is

$$\mu_i = \mu_o \left(\frac{Ti}{To}\right)^{-N} \qquad \text{----------(d')}$$

D. Referring to equation (1), page 85, it follows that if wave motion is to exist, the order of η_t (first term) must be equal to $u_i \eta_x - v_i$. That is to say

$$\sigma \frac{L}{U_r} \triangleq 1, \text{ or } \sigma \triangleq \frac{L}{U_r} \qquad \text{----------(e')}$$

E. In order to satisfy enough boundary conditions, it is necessary to retain the highest order terms in the momentum and energy equations; however at this stage of the analysis it is not known whether the order of the inertia term

and the pressure and body force term should be equated to the viscous term since it is desirable to include the cases of no body force, no pressure gradient, or very slow liquid flow (small inertia term). The determination of the order of $\bar{U}r$ must enter from the boundary condition, in as much as $\bar{U}r$ depends not only on the ablation properties of the material (i.e., depends strongly on μ_i and thus Ti) but also on the gas flow conditions such as the shear force exerted on the liquid surface. When $\partial u_g/\partial y$ and $\partial u_l/\partial y$ are normalized to unit order in equation (o), page 86, it follows that

$$\frac{\mu_g \bar{U}_\infty}{L\delta_g} \; \underline{o} \; \frac{\mu_i \bar{U}_r}{L\delta_l} \qquad \text{----------(f')}$$

F. Similarly, the temperature Ti depends not only on the properties of the ablating material but also on the gas flow conditions, T_∞, $T_{-\infty}$, as well as the gas properties. From equation (m), page 86, with $\partial\theta_g/\partial y$ and $\partial\theta_l/\partial y$ normalized to unit order, it is possible to write

$$\frac{k_g(T_\infty - Ti)}{Le_g} \; \underline{o} \; \frac{k_l(Ti - T_{-\infty})}{Le_l} \qquad \text{-----(g')}$$

G. The order of δ_l and e_l may be determined from examination of the long time stage of ablation. If the fluctuation of temperature due to the wave motion is neglected, the term $\partial\theta/\partial t$ tends to approach zero. An observer on the stagnation point then sees the heat transferred to the liquid through the interface from the gas side partially carried away by the liquid layer flowing downstream and partially conducted through the liquid layer for further melting. In other words, the conduction term in the long time stage is equally as important as the convection term. Since the region near the stagnation point may be approximated by $\partial\theta/\partial x = 0$, (equation t), it follows from equation (j) that

$$\frac{\delta_l}{e_l} \; \underline{o} \; \frac{k_l}{c_{pl}\rho_l L \bar{U}_r e_l^2} \qquad \text{----------(h')}$$

A second relation for the relative order of δ_l and e_l may be obtained by observing that at $T = T_m$ the liquid velocity vanishes; however the temperature layer may extend into the unmelted body. The relative order of the velocity and temperature layers can thus be given as

$$\frac{\delta_l}{e_l} \simeq \frac{Ti - Tm}{Ti - T_{-\infty}} \qquad \text{----------(i')}$$

The 9 equations (a' through i') may be solved algebraically for the 9 unknown reference quantities. The applicable results have been quoted earlier on pages 81 and 82.

LIST OF SYMBOLS

In addition to the parameters quoted on pages 81 and 82, the following notation is used throughout this report:

Subscripts

g Gas (air) stream.

l Liquid (or melted material).

i Interface value.

o Reference value.

Symbols

A Dimensional acceleration.

c_p Specific heat--BTU/lb.^{o}R.

H(X,t) Interface wave function.

k Thermal conductivity--BTU/hr.ft.^{o}R.

L Dimensional length.

$\bar{L}w$ Wave spacing--feet.

Lx Distance from plate leading edge--feet.

P Dimensional pressure.

P_o Stagnation pressure.

Pr Prandtl number--$\mu c_p/k$.

Q Heat flow.

R Dimensional radius of axisymmetric body.

Re Reynolds number - $\rho \bar{U} L_x / \mu$.

T Dimensional temperature.

Ti Interface temperature--^{o}F.

Tm Body softening temperature--^{o}F.

To Reference temperature--^{o}F.

T_∞ Air stream temperature--^{o}F.

$T_{-\infty}$ Initial body temperature--^{o}F.

$\bar{U}, \bar{V}$ Dimensional liquid velocity components.

$\bar{U}w$ Wave velocity--feet per second.

$\bar{U}$ Air stream velocity--feet per second.

X Coordinate along body surface.

Y Coordinate normal to body surface.

$\bar{Y}w$ Wave amplitude--feet.

μ Absolute viscosity--poise.

ρ Density--slug/ft^3.

LIST OF REFERENCES

1. O'KEEFE, J. A. The Origin of Tektites. NASA TN D-490. 1960.

2. BARNES, V. E. Tektites. Scientific American, 205, no. 5:58-65. Nov. 1961.

3. CHAPMAN, D. R. Recent Re-entry Research and the Cosmic Origin of Tektites. Nature, 188, no. 4748:353-355. Oct. 1960.

4. _____. On the Unity and Origin of the Australian Tektites. NASA TM X-54004. 1963.

5. CHAPMAN, D. R., LARSON, H. K., and ANDERSON, L. A. Aerodynamic Evidence Pertaining to the Entry of Tektites into the Earth's Atmosphere. NASA TR R-134. 1962.

6. CHAPMAN, D. R., and LARSON, H. K. The Lunar Origin of Tektites. Presented at the 13th Int'l. Astronaut. Congr., Varna, Bulgaria. Sept. 1962.

7. CHAPMAN, D. R. On the Unity and Origin of Australasian Tektites. Geochim. Cosmochim. Acta, 28, 841-880. 1964.

8. O'KEEFE, J. A. Tektites and Impact Fragments from the Moon. Scientific American, 210, no. 2:50-57. Feb. 1964.

9. _____. Water in Tektite Glass. J. Geophysical Research, 69, no. 17:3701-7. Sept. 1964.

10. KING, E. A., Jr. An Aerodynamically Sculptured Bediasite. J. Geophysical Research, 69, no. 22: 4731-3. Nov. 1964.

11. FLEISCHER, R. L., NAESER, C. W., PRICE, P. B., and WALHER, R. M. Cosmic Ray Exposure Ages of Tektites by the Fission-Track Technique. J. Geophysical Research, 70, no. 6:1491-6. March 1965.

12. HOYTE, A., SENFTLE, F., and WIRTZ, P. Electrical Resistivity and Viscosity of Tektite Glass. J. Geophysical Research, 70, no. 8:1985-94. Apr. 1965.

13. BETHE, H. A., and ADAMS, M. C. A Theory for the Ablation of Glassy Materials. J. A. S., 26, no. 6: 321-8. June 1959.

14. ADAMS, M. C., POWERS, W. E., and GEORGIEV, S. An Experimental and Theoretical Study of Quartz Ablation at the Stagnation Point. AVCO Res. Rept. 57. 1959.

15. GEORGIEV, S., HIDALGO, H., and ADAMS, M. C. On Ablating Heat Shields for Satellite Recovery. AVCO Res. Rept. 65. 1959.

16. _____. On Ablation for the Recovery of Satellites. AVCO Res. Rept. 47. 1959.

17. SUTTON, G. W. The Hydrodynamics and Heat Conduction of a Melting Surface. J. A. S., 25, no. 1:29-32. Jan. 1958.

18. GEORGIEV. S. Unsteady Ablation. AVCO Res. Rept. 94. 1959.

19. ADAMS. M. C. Recent Advances in Ablation. A. R. S. Journal, 29, no. 9:625-632. 1959.

20. FANUCCI, J. B., and LEW, H. G. Effect of Mass Transfer and Body Forces on Two Phase Boundary Layers. General Electric Co., Tech. Inf. Series, Res. Memo. No. 35. Apr. 1959.

21. TELLEP, D. M. The Effect of Vehicle Deceleration on a Melting Surface. Lockheed Missles and Space Div., Tech. Rept. LMSD-48331. Jan. 1959.

22. OSTRACH. S., GOLDSTEIN, A. W., and HAMMAN, J. The Effect of a Deceleration Force on a Melting Boundary Layer. J. A. S., 27, no. 8:626-7. Aug. 1960.

23. _____. Analysis of Melting Boundary Layers on Decelerating Bodies. NASA TN D-1312. July 1962.

24. McCONNELL, D. G. A Study of Transient Melting Ablation About a Decelerating Spherical Body. Ph. D. Thesis, Case Inst. of Tech., Cleveland, Ohio. 1964.

25. OSTRACH, S., and McCONNELL, D. G. Melting Ablation About Decelerating Spherical Bodies. NASA TM X-52053. 1964.

26. CHEN, M. (Private Communication from Ph. D. Thesis to be submitted at a later date.) Case Inst. of Tech., Cleveland, Ohio. 1966.

27. MILES, J. W. The Generation of Surface Waves by Wind. Appl. Mech. Rev., 15, no. 9:685-7. Sept., 1962.

28. FRANCIS, J. R. D. Wave Motions and the Aerodynamic Drag on a Free Oil Surface. Phil. Mag., (7), 45: 695-702. 1954.

29. OSTRACH. S., and KOESTEL, A. Film Instabilities in Two-Phase Flows. A. I. Ch. E. Journal, 11, no. 2: 294-303. March, 1965.

30. FELDMAN, S. On the Hydrodynamic Stability of Two Viscous Incompressible Fluids in Parallel Uniform Shearing Motion. Journal of Fluid Mechanics, 2, Part 4:343-370. 1957.

31. MILES, J. W. The Hydrodynamic Stability of a Thin Film in Uniform Shearing Motion. Journal of Fluid Mechanics, 8, Part 4:593-611. 1960.

32. POPE, A. Wind-Tunnel Testing, 2nd ed. John Wiley & Sons, Inc., New York. 1954.

33. PFEIFFER, J. Ph. The Properties of Asphaltic Bitumen. Elsevier Publ. Co., New York. 1950.

34. Handbook of Chemistry and Physics, 43rd ed. The Chemical Rubber Publ. Co., Cleveland, Ohio. 1962.

35. DUKLER, A. E. M. S. Thesis, University of Delaware, Newark, Delaware, 1949.

36. _____. Ph. D. Thesis, University of Delaware, Newark, Delaware. 1951.

37. KNUTH, E. L. Memo No. 20-85, Jet Propulsion Laboratory, California Institute of Technology, Pasadena, California. 1953.

38. LAIRD, A. D. K. Ph. D. Thesis, University of California, Berkeley, California. 1951.

39. KINNEY, G. L., ABRAMSON, A. E., and SLOOP, J. L. Nat. Adv. Comm. Aeronaut. Rept. 1087. 1952.

40. BRAUER, H. VDI Forsch, 22:457. 1956.

41. JAKOB, M., and HAWKINS, G. A. Elements of Heat Transfer, 3rd ed. Wiley & Sons, Inc. 1957.